AD-A210 917

DYNAMIC WATER WAVE PRESSURES ON A RECURVED MODEL SEAWALL

DTIC
ELECTE
AUG 0 8 1989
S D
D

A Thesis

by

GREGORY ROSS RISMILLER

Submitted to the Office of Graduate Studies of
Texas A&M University
in partial fulfillment of the requirements for the degree

MASTER OF SCIENCE

DISTRIBUTION STATEMENT A
Approved for public release
Distribution Unlimited

August 1989

Major Subject: Ocean Engineering

89 8 04 050

DYNAMIC WATER WAVE PRESSURES ON A RECURVED MODEL SEAWALL

A Thesis

by

GREGORY ROSS RISMILLER

Submitted to the Office of Graduate Studies of
Texas A&M University
in partial fulfillment of the requirements for the degree

MASTER OF SCIENCE

August 1989

Major Subject: Ocean Engineering

DYNAMIC WATER WAVE PRESSURES ON A RECURVED MODEL SEAWALL

Accesion For
NTIS CRA&I ☑
DTIC TAB ☐
Unannounced ☐
Justification
By per form 50
Distribution /
Availability Codes
Dist | Avail and/or Special
A-1

A Thesis

by

GREGORY ROSS RISMILLER

Approved as to style and content by:

Jerry L. Machemehl
(Chair of Committee)

John M. Klinck
(Member)

QUALITY INSPECTED 4

Robert E. Randall
(Member)

J.T.P. Yao
(Head of Department)

August 1989

ABSTRACT

Dynamic Water Wave Pressures on a Recurved Model Seawall.

(August 1989)

Gregory Ross Rismiller, B.S., Virginia Polytechnic Institute and State University;

Chair of Advisory Committee: Dr. Jerry L. Machemehl

The dynamic pressures acting on a 1:5 scale recurved model seawall caused by breaking water waves were investigated. The magnitude, location and distribution of the shock and secondary pressures were determined from physical experiments and found to be dependent on breaking wave height, incident wave height, and water depth. During the experiment, the water depth and the incident wave characteristics of wave period and wave height were varied. As the breaking wave height and incident wave height increased, the magnitude of the shock and secondary pressure increased. Shock pressures as great as 3.72 kN/m^2 were recorded, while a change in water depth of 0.01m caused a mean pressure increase of approximately 0.09 kN/m^2. The wave form which caused the greater shock pressures was examined and found to have a relatively large breaking height and steepness, but does not entrap a large quantity of air. The secondary pressures on the upper three transducers consistently showed a negative pressure, the largest value being -1.2 kN/m^2. It was determined that a suction formed as the wave surged past these transducers producing negative pressures.

The experimental results were also compared with several vertical wall shock pressure formulas which are used to predict the shock pressure on a recurved wall. Minikin's formula came closest in agreement to the measured shock pressures. Other formulas predicted values on the order of 4-100 times greater than the measured values.

ACKNOWLEDGEMENT

The author gratefully acknowledges those who contributed to this study. A special note of gratitude is extended to Dr. J. L. Machemehl whose advice, encouragement and support is greatly appreciated.

Messrs. Marty Krafft and Arun Duggal provided able and willing assistance in electronics design, data acquisition and instrumentation. Mr. Krafft's knowledge in all areas of electronic equipment and data aquisition was indispensible. LT Joseph Hedges' advice and help with finding and eliminating instrumentation and procedural problems is greatly appreciated.

A note of thanks is due to the U. S. Navy Civil Engineer Corps for giving the author the opportunity to experience college life again, increase his knowledge and gain new insight into the ocean engineering field.

And finally a special note of thanks is due to the author's wife, Susan, for her continual support and endurance throughout the preparation of this report and eighteen months of graduate study.

TABLE OF CONTENTS

TABLE OF CONTENTS - Continued

LIST OF TABLES

LIST OF FIGURES

LIST OF FIGURES - Continued

LIST OF FIGURES - Continued

CHAPTER I

INTRODUCTION

As a breaking wave contacts the face of a seawall, it causes an initial shock (or impact) pressure of large magnitude and short duration immediately followed by a secondary (or surge) pressure of lesser magnitude and longer duration. There is no single formula used for determining the shock pressures, hence there are no specific guidelines for the design of recurved seawalls (Fig. 1) subjected to these dynamic pressures. It is assumed that the dynamic pressures on a recurved wall follow existing vertical wall pressure formulas.

The purpose of this study was to analyze the dynamic pressures on a recurved seawall caused by breaking waves. This research was conducted with the following specific objectives:

1. To examine the magnitude of the shock and secondary pressures on a recurved wall,

2. To establish the location of the maximum dynamic pressure,

3. To examine the wave form that creates the maximum shock pressure, and

4. To examine the validity of theoretical and empirical formulas.

The citations on the following pages follow the style of the *Journal of Waterway, Port, Coastal, and Ocean Engineering*, ASCE.

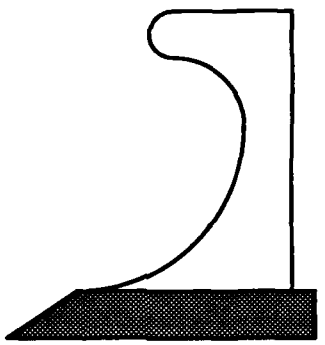

FIG. 1.- Recurved Wall

Impact pressures have been studied extensively with regard to vertical walls, but it has been only in the last decade that research has been conducted with recurved walls. It is extremely difficult to formulate analytical solutions to the problem of breaking waves on a seawall, and therefore it was necessary to rely on scale model tests. The data obtained for the dynamic pressures in this study were compared to the results of others only by use of their theoretical formulas and no attempt was made to describe the dynamic pressures mathematically.

The research was conducted by experiment in a two-dimensional wave flume, using a model recurved seawall fixed with transducers to measure the dynamic pressures. Twenty four tests were conducted with model wave heights ranging from 0.058 to 0.098 m, and model wave periods ranging from 1.5 to 2.25 sec.

CHAPTER II

LITERATURE REVIEW

Wave Breaking on a Vertical Wall

Numerous investigators, Carr (3), Garcia (5), Kamel (10), Kirkgoz (12), Minikin (15), Nagai (17), Ross (20), and Rundgren (22) have collected laboratory and field data to determine the magnitude and duration of impact pressures on vertical walls. Test results showed extreme variations.

Bagnold (1) theorized that the short duration shock pressures resulted from the rapid compression of a thin air pocket trapped between the face of a breaking wave and the wall. Ross (20,21), and Kirkgoz (12) theorized that shock pressures existed without entrapped air. According to Ross (20,21), the wave must break directly on the wall rather than breaking in front of the wall, or not quite breaking, and have its front face parallel to the wall at the instant of impact to produce the greatest shock pressures. Mitsuyasu (16), Richert (19), and Rundgren (22) agreed with Bagnold that shock pressures occur only when air is enclosed between the wave and the wall.

Kamel (10,11) using an elastic wave theory suggested that measured maximum impact pressures are eight times smaller than theoretical maximum pressure due to the presence of an air pocket in the breaker,

or between the wave and the wall at impact, or both. Kamel attained the theoretical value with the absence of the air pocket.

Debate still exists concerning the relative importance of these shock pressures to the actual design of a seawall. A common opinion among many engineers is that shock pressures of such short duration should not be used for establishing design loadings for sliding or overturning. Carr (3) and Ross (20,21) believed the lower dynamic secondary pressures, which last longer, were more important. The secondary pressure was caused by the motion of the water at the wall during runup and by the static head of water. At the time of maximum runup the static head is the greatest on the wall and the water particles have zero velocity. During downrush, the pressure decreases to zero as the water level falls. Rundgren (22) theorized, and Garcia (5) agreed, that the secondary pressure is on the order of magnitude of the clapotis or nonbreaking wave that is reflected from a wall. The clapotis pressure is also caused by a combination of static head and velocity of the water particles. Therefore, the secondary pressure can be predicted from developed wave pressure equations.

As for the location of the maximum shock pressure and the vertical distribution of simultaneous pressures, many different results and opinions (5,12,15,17,22) are available. In design, the still water level (SWL) is normally regarded as being the probable location for the maximum shock pressure, regardless of the bottom slope and wave properties.

The most widely used formula for predicting shock pressure on vertical walls due to breaking waves was derived by Minikin (15). The pressure distribution is shown in Fig. 2. Minikin theorized that the maximum force acts at the SWL and then decreases parabolically from SWL to zero at a distance of 1/2 the breaker height above and below the

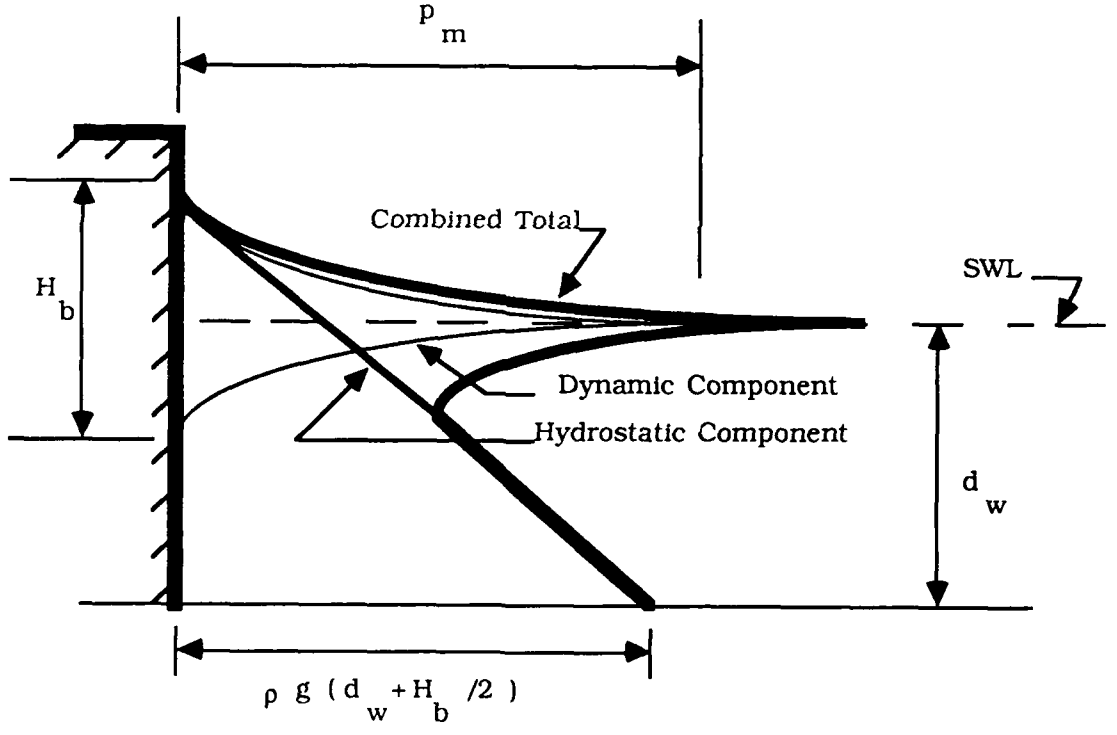

FIG. 2.- Minikin Pressure Distribution
[After U.S. Army Coastal Engineering Research Center (23)]

SWL. There are however certain limitations to this equation. Minikin's equation is not dimensionally homogeneous and is very dependent on the bathymetry in front of the structure. The dynamic pressure computed is considered to be of a static nature. The dynamic pressure is added to the hydrostatic pressure to obtain the total maximum pressure on a structure. This may result in large impractical cross sections of the structure especially for those to be located on flat bottoms. Gouda (6) used hydrodynamic theory to agree with Minikin's theory of maximum pressure occurring at SWL, but differed in that the distribution is a parabolic curve above SWL and hyperbolic below SWL.

Many investigators, Garcia (5), Kirkgoz (12), Minikin (15), Nagai (17), and Rundgren (22), have suggested widely varying positions for the point of maximum pressure, depending upon the particular wave and beach conditions. Kirkgoz (12) suggests this location is above SWL, with the vertical distribution described by a parabolic curve fitted between maximum and bottom values. Above the location of the maximum pressure, the distribution is linear, diminishing to zero at the top of the wave.

Experiments by Garcia (5) showed a wide scatter of shock pressures for the same wave condition and maximum shock pressures occuring mostly between the SWL and the breaking crest height. The parabolic distribution proposed by Minikin closely approximated Garcia's actual distribution of maximum shock pressures.

The impact pressure at the foot of the wall has been the subject of some controversy. Nagai (17) found it to be zero, while Rundgren (22) reported the maximum shock as acting at this point. It is almost certain that the wide range of variation in pressures measured at this point is due to various breaker types used in the studies (12).

Richert (19) and Kirkgoz (12) found that the most severe shock pressures occurred with a 1/10 beach slope. Kirkgoz suggested that it is only over a limited range of intermediate beach slopes (between 1/8 and 1/14) that the most severe pressures are produced. In general, all investigators have shown that maximum shock pressure on vertical walls is a function of deepwater wave steepness and beach slope. A summary of the formulas derived by various investigators are shown in Table 1.

TABLE 1.- Summary of Formulas

Investigator	Formula	Units
Bagnold (1)*	$p_m = 0.54\ \rho \frac{H}{D_T} C^2 + p_0$	(lb/ft^2)
Minikin (15)	$p_m = 101\ \gamma\ (d_w + D)\ \frac{d_w}{D}\ \frac{H_b}{L_D}$	(lb/ft^2)
Nagai (17)	$p_m = 300 \left(0.051\ \frac{d_w^2}{D}\ \frac{H}{L}\right)^{1/3}$	(g/cm^2)
Garcia (5)	$p_m = 50\ (\gamma)^{2/3}\ E_0^{1/3}$	(lb/in^2)
Kamel (10)	$p_m = \left(\frac{\rho_{sw}\ C_{sw}}{\rho\ C_w + \rho_{sw}\ C_{sw}}\right) \rho_w\ C$	(lb/ft^2)

*D_T represents the thickness of the entrapped layer of air, which is very difficult to measure, and is beyond the scope of this research.

Wave Breaking on a Recurved Wall

For recurved walls, the U.S. Army Coastal Engineering Research Center (23) suggests the maximum shock pressure and its distribution should be determined by vertical wall formulas. Grace and Carver (7) conducted experiments on a vertical, recurved, and modified recurved (with a horizontal lip) walls in monochromatic waves. They concluded that the greatest shock pressures ocurred at the SWL for the vertical and recurved walls, but at the lower face of the horizontal lip for the modified recurved wall. They also determined that there was no significant difference in the magnitude or duration of

the secondary pressure on wall geometry, for vertical, recurved, or modified recurved walls.

Berkeley Thorn and Roberts (2) report that there are limitations in using regular waves when designing for overtopping. Overtopping may increase if irregular waves of sufficient wave height equal to the wave height of regular waves are used in an experimental study. Heimbaugh, et al. (8) conducted overtopping experiments with recurved walls with a stepped foreshore on a riprap base using irregular waves. They found that the maximum shock pressures, depending on the water depth, occurred at the vertex of the small curvature on the wall, or on the stepped foreshore.

Berkeley Thorn and Roberts (2) present a standard design for recurved seawalls, but according to Owen (18) these are only a few broad guidelines and the necessary quantitative information is lacking. Owen further states that model studies are required for a proper evaluation of their performance.

CHAPTER III

THEORETICAL DEVELOPMENT

Waves breaking on a structure are an impact problem. Using Newton's second law, an impulse-momentum relation may be written:

$$F = m\,a = \frac{d(mu)}{dt} \tag{1}$$

Assuming the mass remains constant and can be replaced by the product of the mass density, ρ, area, A, and a length, ℓ, and further assuming that the force, F, may be expressed in terms of an average pressure, p, acting over an area, A, Eq. 1 can be written as

$$p\,dt = d(\rho\,\ell\,u) \tag{2}$$

When pressures are not excessively high, the effects of the compressibility of a liquid are normally negligible. According to Kamel (11) and Kirkgoz (12), if there are large pressure differences, such as shock pressures, the elasticity of liquids may need to be taken into consideration.

In a compressible fluid the bulk modulus of elasticity, E, is given as

$$E = \frac{\frac{dp}{d\ell}}{\frac{}{\ell}} = \frac{dp}{\frac{d\rho}{\rho}} \tag{3}$$

Proceeding with Eq. 2

$$\frac{p}{\ell} dt = u \, d\rho + du \tag{4}$$

and substituting $d\rho$ from Eq. 3 into Eq. 4 gives

$$\frac{p}{\ell} dt = u \frac{\rho}{E} dp + \rho \, du \tag{5}$$

The equation of motion for a steady-state flow is

$$- dp = \rho \, u \, du \tag{6}$$

and on substituting Eq. 6 into Eq. 5

$$\frac{p}{\ell} dt = - \frac{\rho^2}{E} u^2 \, du + \rho \, du \tag{7}$$

Assuming all of the momentum of the mass is lost between the time the impact pressure first begins to act and the time, t_m, when the pressure reaches its peak value, p_m (Fig. 3), then during this time interval, the velocity, u, changes from u_b, the breaking velocity, to zero. Eq. 7 becomes

$$\int_0^{t_m} \frac{p}{\ell}\, dt = -\int_{u_b}^{0} \frac{\rho^2}{E}\, u^2\, du + \int_{u_b}^{0} \rho\, du \qquad (8)$$

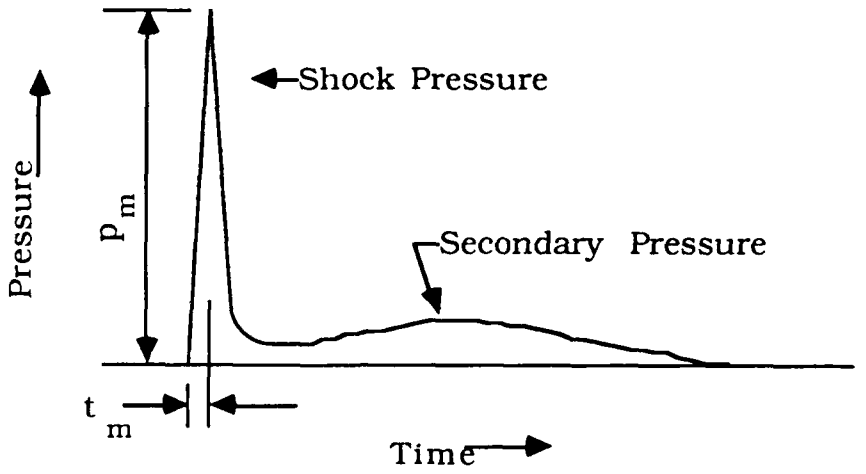

FIG. 3.- Typical Pressure-Time Curve
[After Kirkgoz (12)]

The relationship between p and t may be assumed to be linear between the time when pressure first begins to act, t = 0, and when pressure is maximum, $t = t_m$. Then,

$$\frac{1}{2}\, \frac{p_m}{\ell}\, t_m = \frac{\rho^2}{3E}\, u_b^3 - \rho\, u_b \qquad (9)$$

Rewriting Eq. 9, the sign changes on the right-hand side because the interest is on the pressure exerted against the wall,

$$p_m \; t_m = 2 \; \ell \; (\rho \; u_b - \frac{\rho^2}{3E} \; u_b^3) \qquad (10)$$

For water wave motion, the second term inside the parentheses in Eq. 10 is very small compared with the first term. Ignoring the elasticity term,

$$p_m \; t_m = 2 \; \ell \; \rho \; u_b \qquad (11)$$

The parameters on the left side of Eq. 11 may be determined from pressure measurements, while u_b may be found from breaker measurements. The length, ℓ, may be evaluated using mass density of water, ρ.

CHAPTER IV

METHODOLOGY

The phenomena of a breaking wave on a seawall is not describable by mathematical equations, and therefore it is necessary to rely on scale model tests. The modeling technique for this study was according to Froude's scaling law. The recurved test wall model is a 1:5 scale model of the recurved section of the proposed wall in Virginia Beach, Virginia (8). Scale selection was based on the test facilities, the capabilities of the wave generation system, and the pressure transducers used to measure the data.

Dimensional Analysis

The magnitude of shock pressures varies with the form of the waves as they make contact with the seawall. Factors which influence the magnitude and duration of these pressures are wave dimensions, bottom slope, concentration of entrained air in the water, and the pressures in air pockets trapped between the wave and the wall at contact.

Following Hudson, et al. (9), the flow over the recurved wall can be assumed a function of :

depth of water at breaking = d_b

modulus of elasticity of the water = E

bulk modulus of the seawall = E_{sw}

acceleration due to gravity = g

wave height at breaking = H_b

adiabatic constant of air = k

pressure intensity on the wall = p

atmospheric pressure = p_o

mass density of the seawall = ρ_{sw}

mass density of the water = ρ

wave period = T

angle of bottom slope = θ

angle of incident wave attack = β

wave length = L

surface tension of the water = σ

Using the Buckingham pi theorem, the above parameters can be put into dimensionless form. The viscous shear forces are negligible compared to gravity, inertia, pressure, and elastic forces. Also the angle of bottom slope and angle of incident wave attack is considered insignificant in these experiments; therefore they will be dropped. After rearranging and combining terms, a functional relationship for shock pressure is

$$\frac{p-p_o}{p_o} = f\left[\frac{H_b}{d_b}, \frac{(gH_b)^{1/2}T}{d_b}, \frac{\sigma T^2}{\rho H_b d_b^2}, k, \left(\frac{E}{\rho}\right)^{1/2}\frac{T}{d_b}, \left(\frac{E_{sw}}{\rho_{sw}}\right)^{1/2}\frac{T}{d_b}, \frac{\rho}{\rho_{sw}}\right] \qquad (12)$$

This functional relationship will be used to correlate the resulting test data in the form of dimensionless plots.

CHAPTER V

EXPERIMENTAL APPARATUS AND EQUIPMENT

The model testing was performed in a 2-dimensional glass walled wave flume, 120 ft (36.6m) long, 2 ft (0.61m) wide, and 3 ft (0.91m) deep (Fig. 4), at the Hydromechanics Laboratory, Texas A&M University. Breaking conditions were created by the use of a 1:10 beach slope in front of the test wall. The wall was constructed of plexiglass ribs and sheet metal face, fitted with pressure transducers spaced vertically along the wall centerline. A schematic diagram of the recurved test wall with pressure transducer locations is shown in Fig. 5. Fig. 6 shows photographs of front, and rear views of the test wall. The transducers were Statham PA285TC Absolute Pressure Transducers, each with pressure range of 0-50 psia (0-344.75 kN/m^2), with 100% overpressure capability, and natural frequency of 8,000 Hz (Fig. 7).

The waves were generated by a Seasim wave making system (Fig. 8) consisting of a Programable Spectrum Random Signal Generator, Servo Control Amplifier LSC 24-48, and a paddle type Rolling Seal Wavemaker RSW 30-60. Wave characteristics were measured with a Seasim Auto Compensating Wave Height Gauge, and two wave probes. One wave probe was placed in the reach of the flume with a horizontal bottom. The second wave probe was placed 20.32 cm in front of the test wall (See Fig. 4).

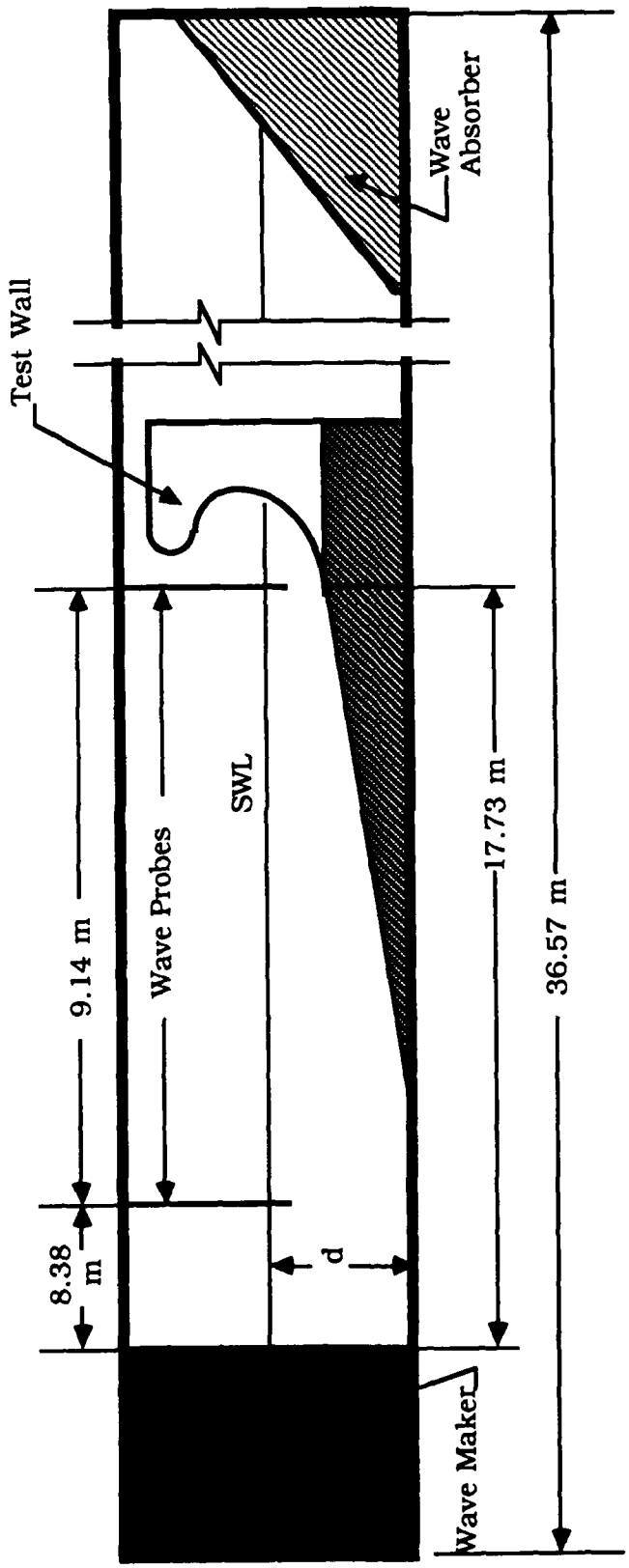

Fig. 4.- Wave Flume and Test Equipment
(not to scale)

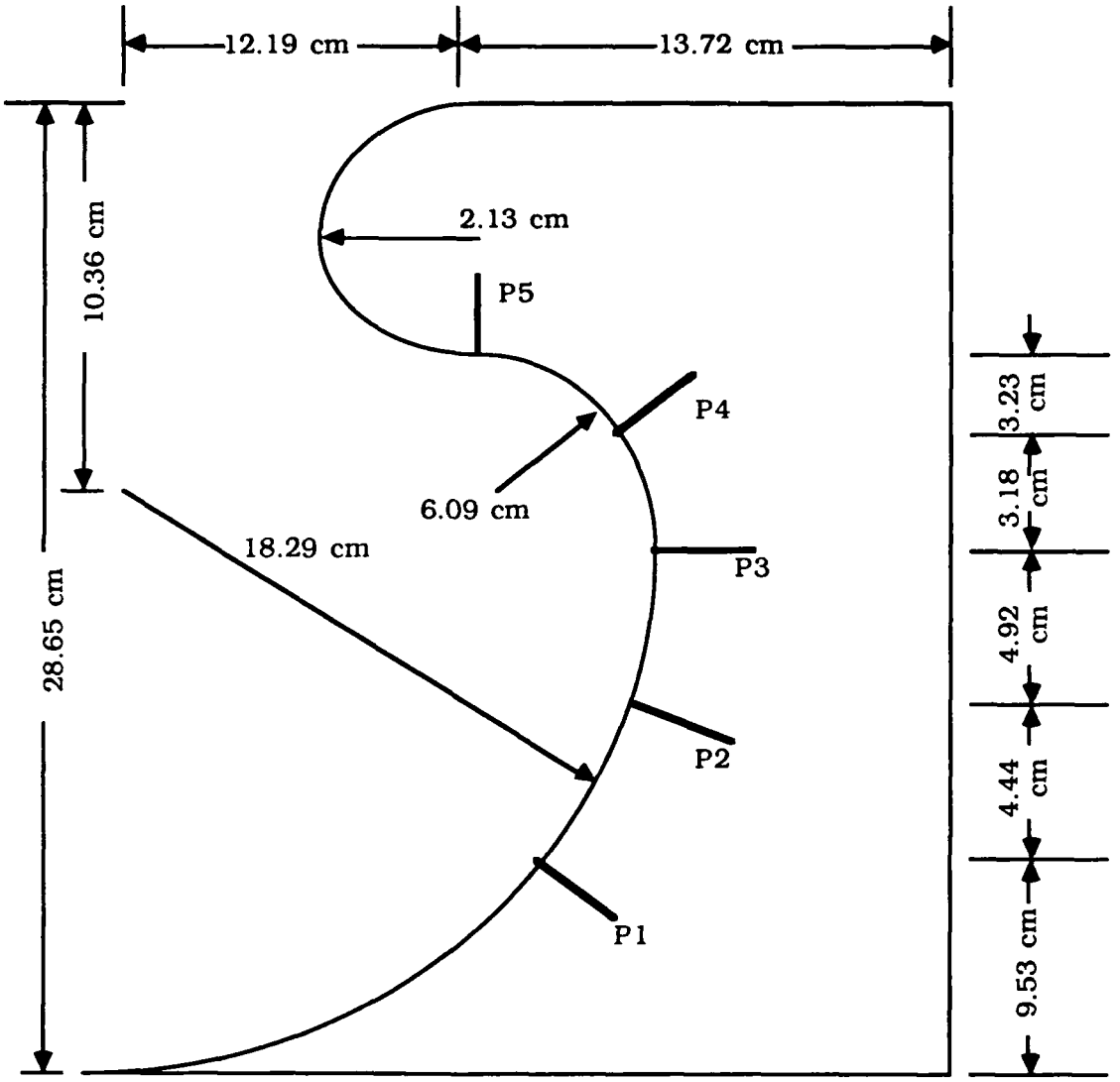

FIG. 5.- Test Wall
(not to scale)

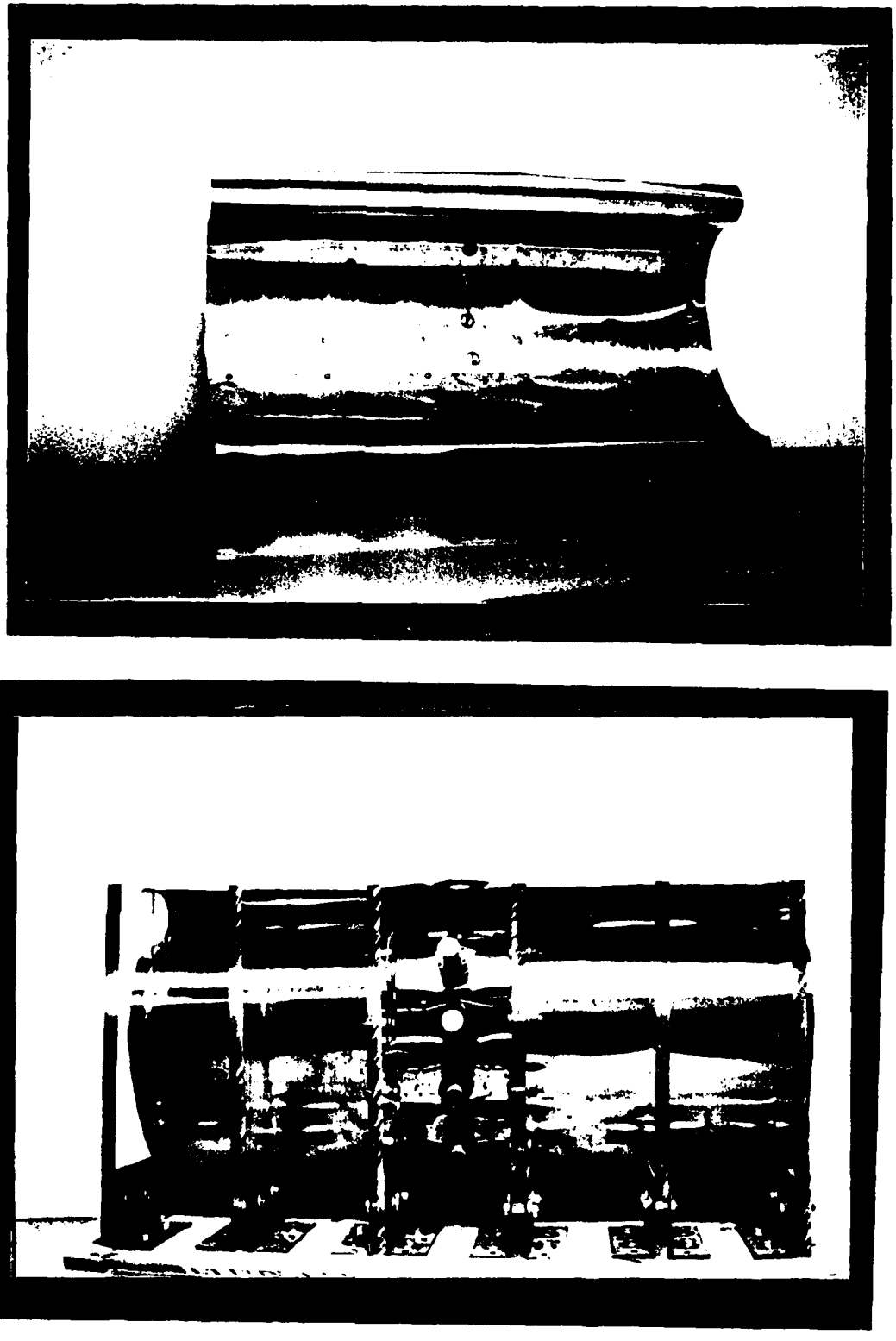

FIG 6.- Front and Rear View of Test Wall

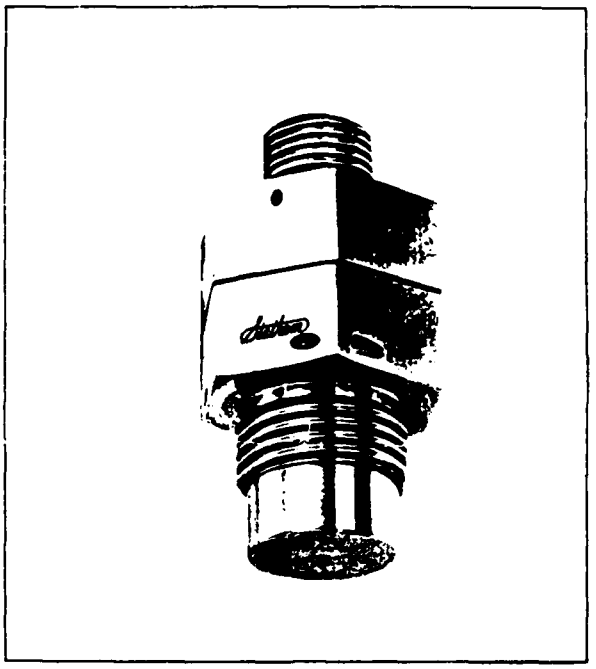

FIG 7.- Statham PA28FTC Pressure Transducer

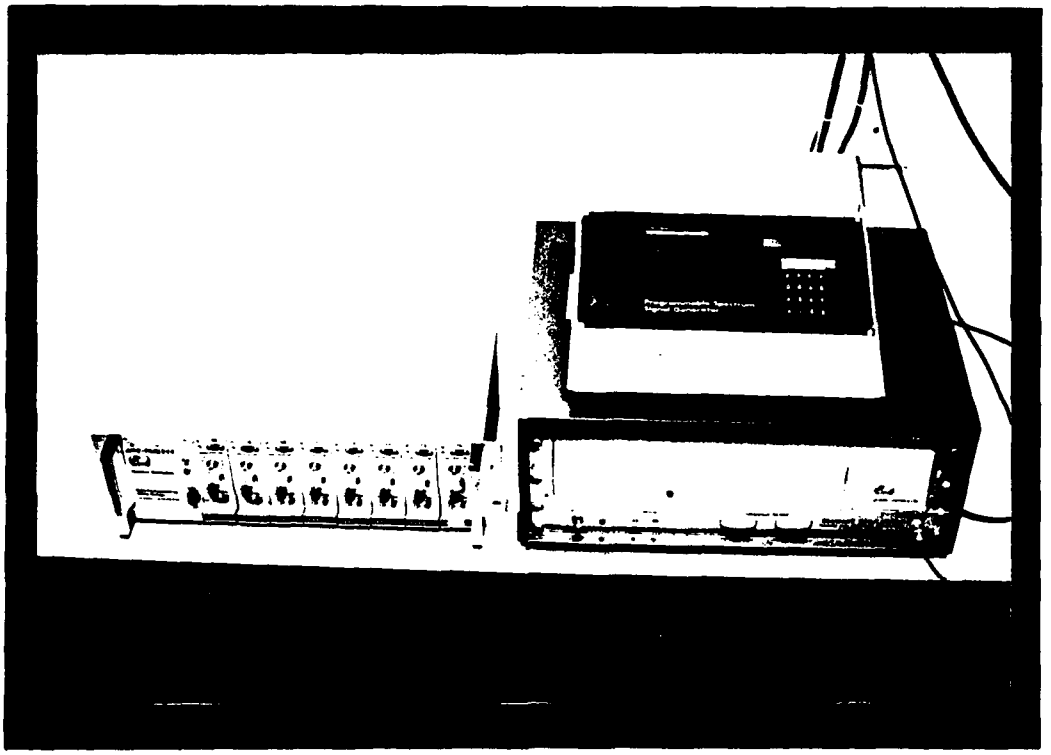

FIG 8.- Seasim Wavemaking System

The wave height and pressure measurements were recorded with a Hewlett-Packard Data Acquisition System (Fig. 9). The system consisted of an HP 3852A Data Acquisition/Control Unit, HP 44702B High Speed Voltmeter, HP 44711A FET Multiplexer, and an HP 9000 Series 300 Computer. Various computer programs were utilized to calibrate the instruments and collect the data. "MULTI_CAL" (13) and "MULTI_SCAN" (14) were used to calibrate the wave probes and zero the pressure transducers. To collect the data, "FAST_SCAN" (4) was used.

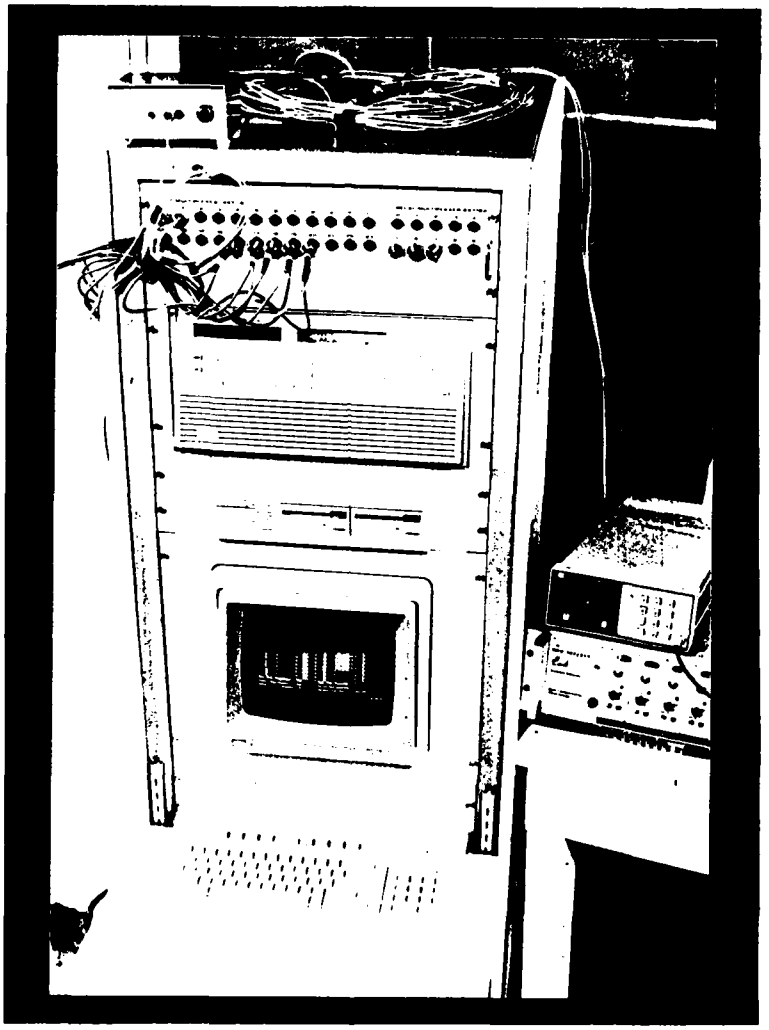

FIG 9.- Hewlett-Packard Data Aquisition System

CHAPTER VI

EXPERIMENTAL PROCEDURE

Prior to the test program, sample waves were run to determine the best range of wave characteristics. Originally, it was planned to collect data from the first three breaking waves. However, the sample waves showed that there was too much disturbance from wave reflection and splash to use the first three breaking waves, especially for periods less than 1.5 seconds. Therefore, data was obtained from the first breaking wave in each run.

The test program consisted of 24 test series with three test runs per series. The SWL had one of two values 0.61 m, and 0.62 m. The test program is shown in Table 2. The wave probe in the reach of the flume measured the wave height, H. According to Small Amplitude (or Airy) Wave Theory (23), the wavelength, L, celerity, C, and deep water wave height, H_o, and length, L_o, were calculated using the following formulas:

$$L = \frac{gT^2}{2\pi} \tanh\left(\frac{2\pi d}{L}\right) \tag{13}$$

$$C = \frac{L}{T} \tag{14}$$

$$H_o = H\left(\tanh\left(\frac{2\pi d}{L}\right)\left(1+\frac{\left(\frac{4\pi d}{L}\right)}{\sinh\left(\frac{4\pi d}{L}\right)} \right)\right)^{1/2} \qquad (15)$$

$$L_o = \frac{gT^2}{2\pi} \qquad (16)$$

The gauge adjacent to the test wall measured the wave height at breaking, H_b. After data from the breaking wave were recorded, the wave maker was stopped, the water in the flume was allowed to calm before the next run, and the face of the test wall was washed with flume water to reduce any thermal drift effects.

The wave probes were calibrated in the static mode. After every series, the probes were checked and recalibrated if necessary. The pressure transducers were calibrated using the manufacture's linear calibration factor. The transducers were checked after each series and rezeroed if necessary.

TABLE 2.- Test Program

Test Program				
Test Series	Test Run	Water Depth, d (m)	Period, T (sec)	Wave Maker Amplitude Gain
1	1	0.61	1.50	4.00
	2	0.61	1.50	4.00
	3	0.61	1.50	4.00
2	1	0.61	1.50	4.75
	2	0.61	1.50	4.75
	3	0.61	1.50	4.75
3	1	0.61	1.50	5.50
	2	0.61	1.50	5.50
	3	0.61	1.50	5.50
4	1	0.61	1.75	4.00
	2	0.61	1.75	4.00
	3	0.61	1.75	4.00
5	1	0.61	1.75	4.75
	2	0.61	1.75	4.75
	3	0.61	1.75	4.75
6	1	0.61	1.75	5.50
	2	0.61	1.75	5.50
	3	0.61	1.75	5.50
7	1	0.61	2.00	4.00
	2	0.61	2.00	4.00
	3	0.61	2.00	4.00
8	1	0.61	2.00	4.75
	2	0.61	2.00	4.75
	3	0.61	2.00	4.75
9	1	0.61	2.00	5.50
	2	0.61	2.00	5.50
	3	0.61	2.00	5.50
10	1	0.61	2.25	4.00
	2	0.61	2.25	4.00
	3	0.61	2.25	4.00
11	1	0.61	2.25	4.75
	2	0.61	2.25	4.75
	3	0.61	2.25	4.75
12	1	0.61	2.25	5.50
	2	0.61	2.25	5.50
	3	0.61	2.25	5.50

TABLE 2.- Continued

Test Program				
Test Series	Test Run	Water Depth, d (m)	Period, T (sec)	Wave Maker Amplitude Gain
13	1	0.62	1.50	4.00
	2	0.62	1.50	4.00
	3	0.62	1.50	4.00
14	1	0.62	1.50	4.75
	2	0.62	1.50	4.75
	3	0.62	1.50	4.75
15	1	0.62	1.50	5.50
	2	0.62	1.50	5.50
	3	0.62	1.50	5.50
16	1	0.62	1.75	4.00
	2	0.62	1.75	4.00
	3	0.62	1.75	4.00
17	1	0.62	1.75	4.75
	2	0.62	1.75	4.75
	3	0.62	1.75	4.75
18	1	0.62	1.75	5.50
	2	0.62	1.75	5.50
	3	0.62	1.75	5.50
19	1	0.62	2.00	4.00
	2	0.62	2.00	4.00
	3	0.62	2.00	4.00
20	1	0.62	2.00	4.75
	2	0.62	2.00	4.75
	3	0.62	2.00	4.75
21	1	0.62	2.00	5.30
	2	0.62	2.00	5.30
	3	0.62	2.00	5.30
22	1	0.62	2.25	4.00
	2	0.62	2.25	4.00
	3	0.62	2.25	4.00
23	1	0.62	2.25	4.75
	2	0.62	2.25	4.75
	3	0.62	2.25	4.75
24	1	0.62	2.25	5.30
	2	0.62	2.25	5.30
	3	0.62	2.25	5.30

Durations of shock pressures are characteristically less than 0.01 seconds. Therefore, to aquire a record of the pressure response, a high sampling rate was imperative. It was determined that a 1000-Hz sampling rate was satisfactory. Due to data storage capabilities, the actual data aquisition interval was 3 seconds. A summary of the wave data collected is shown in Table I-1.

Pressure versus time plots were then prepared from the raw data for each transducer, for each run. From these plots, shock pressure, p_m, maximum shock pressure per series, p_{max}, and secondary pressure, p_s, were determined. The results of all plots are tabulated in Appendix I.

CHAPTER VII

DISCUSSION OF RESULTS

The functional relationships show that the extremely complex interactions of the water, compressed air, and capillary forces create problems in determining approximate equations for correcting model results to minimize errors in transforming the results to prototype quantities. Therefore, all of the results were kept in model quantities for analysis.

Shock and Secondary Pressure

Fig. 10 and Fig. 11 show pressure-time plots of the shock and secondary pressures for Series 23, Transducer 1, and Series 20, Transducer 4 respectively. Pressures on Transducer 1 and Transducer 2 were very similar in shape and size, as expected. Only in Series 1 and 8 were pressures greater on Transducer 2 than Transducer 1. However, results from Transducers 3 through 5 were very unexpected. As seen in Fig. 11, there is an initial shock pressure. Each transducer experienced this to some degree. The secondary pressure is negative, sharply at first, then gradually increasing to zero. The negative secondary pressure occurred on Transducers 3 through 5 on every run.

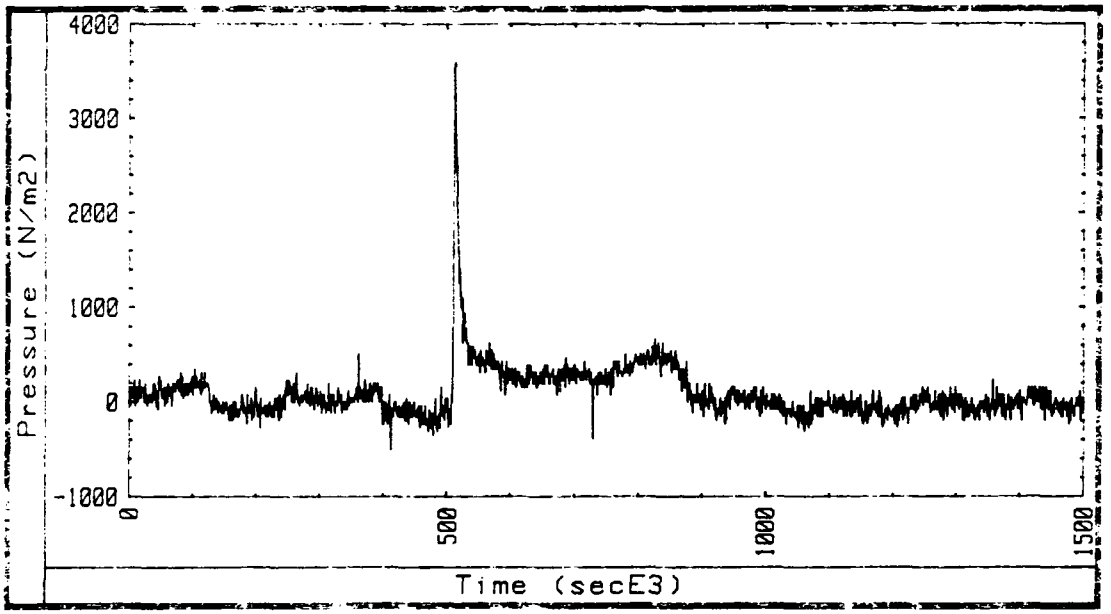

FIG. 10.- Pressure-Time Plot, Series 23, Transducer 1

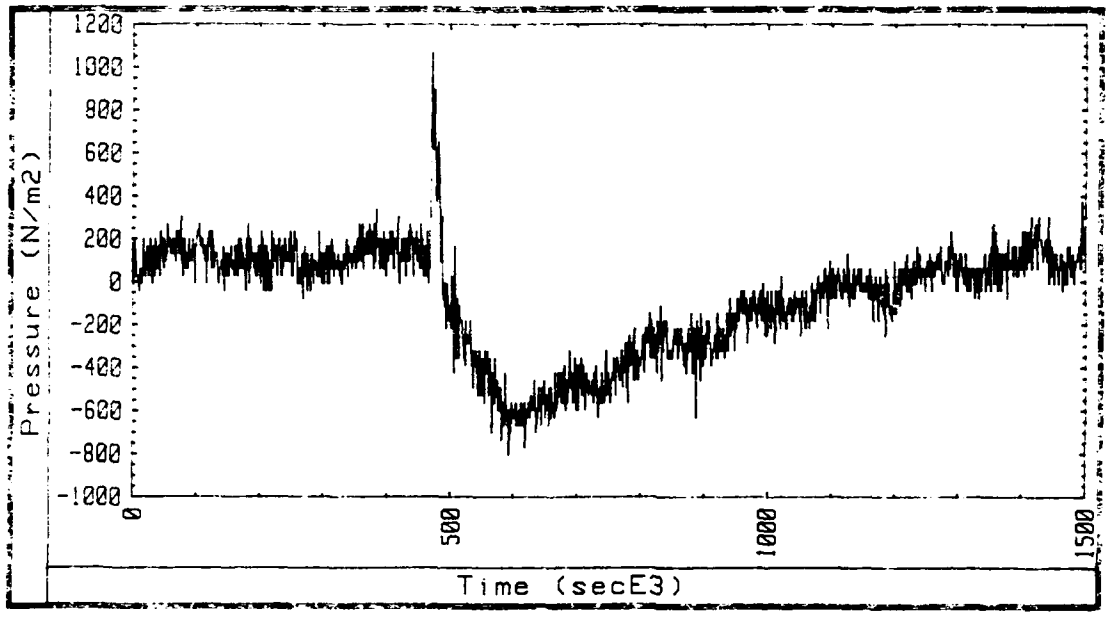

FIG. 11.- Pressure-Time Plot, Series 20, Transducer 4

The shock pressure data recorded on each transducer is presented in Table I-2. It can be seen that in general, as wave height, and water depth increased, the magnitude of the shock pressure increased. It can also be seen that a great variation of magnitude of the shock pressure occurs even between runs of the same wave characteristic. This is very common due to the irregularity of the impact phenomena. A missing shock pressure value in Table I-2 does not necesssarily mean there was no shock pressure on that transducer. The shock pressure was so small, it was on the order of the noise reading and not discernable from the noise.

Table I-3 shows the secondary pressure data collected. The magnitude of the secondary pressures was not as varied as the shock pressures. As expected, the secondary pressure increased as the size of the wave increased and the maximum values (absolute values) occurred at Transducer 3, located at the middle of the curvature of the wall, and at Transducer 5, located at the top of the wall. The reason for the negative pressure must be due to the curvature of the wall. After impact, as the wave surges up the face of the wall, there is only tangential velocity around the curve. The velocity is so great, a suction forms causing the transducer diaphram to experience a negative pressure.

Comparison

As presented in Chapter II, there are numerous formulas to predict the magnitude of the shock pressure for a vertical wall, but none for a recurved wall. Table 3 shows a comparison of the measured maximum shock pressure for each series with values computed using formulas from Minikin, Nagai, Garcia, and Kamel. The values from Table 3 are plotted in Figures 12-15.

The Minikin values (Fig. 12) came very close to the measured values, generally on the high side. The only exception occurred during Series 15, and Series 22-24. During Series 22-24, H and H_b decreased slightly. Minikin's formula is a function of H_b, therefore the value decreases. The same happens to Nagai's values (Fig. 13) during the last three series due to the fact that Nagai's formula is a function of H. Garcia's values (Fig. 14) are functions of deepwater wave energy, E_o. The deepwater wave energy is equal to

$$E_o = \frac{1}{8} \rho g H_o^2 L_o \qquad (17)$$

and these values are much larger than the measured values. Kamel's theoretical maximum shock pressure values are shown in Figure 15. They are a measure of the pressure without an air pocket and a function of wave celerity, C. These values are extremely large.

TABLE 3.- Comparison of Shock Pressure

Maximum Shock Pressure (p_{max}) On Wall					
Test Series	Measured (kN/m^2)	Minikin (kN/m^2)	Nagai (kN/m^2)	Garcia (kN/m^2)	Kamel (kN/m^2)
1	0.97	2.19	3.40	64.68	2676.71
2	1.31	2.26	3.59	72.05	2676.71
3	1.79	2.73	3.78	80.28	2676.71
4	1.66	1.87	3.14	67.45	2839.93
5	0.69	2.32	3.33	76.65	2839.93
6	2.21	2.88	3.53	85.95	2839.93
7	1.45	1.44	2.67	70.69	2933.78
8	1.38	1.71	2.83	79.50	2933.78
9	1.21	1.54	3.03	90.60	2933.78
10	1.14	1.19	2.40	70.72	3011.30
11	1.10	1.28	2.52	78.13	3011.30
12	1.24	1.50	2.63	85.21	3011.30
13	1.79	2.82	3.78	67.39	2717.52
14	1.66	2.54	4.02	75.87	2717.52
15	3.72	3.10	4.23	83.91	2717.52
16	1.86	2.56	3.30	70.19	2876.65
17	3.03	2.53	3.51	79.22	2876.65
18	2.34	2.99	3.70	87.77	2876.65
19	1.66	1.91	2.97	72.99	2986.82
20	1.52	2.26	3.14	81.67	2986.82

TABLE 3.- Continued

Maximum Shock Pressure (p_{max}) On Wall					
Test Series	Measured (kN/m^2)	Minikin (kN/m^2)	Nagai (kN/m^2)	Garcia (kN/m^2)	Kamel (kN/m^2)
21	1.66	2.44	3.39	95.32	2986.82
22	1.72	1.44	2.62	70.72	3064.35
23	3.65	1.59	2.84	83.02	3064.35
24	2.41	1.78	2.92	87.57	3064.35

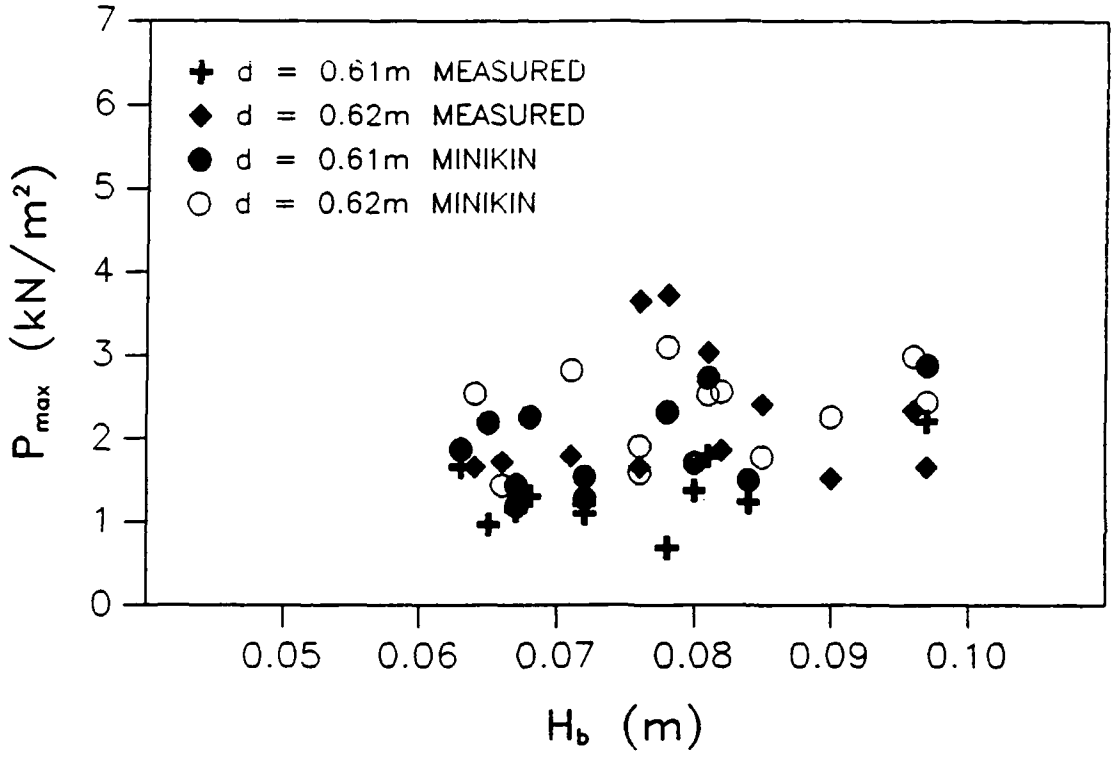

FIG. 12.- Maximum Shock Pressure Versus Breaking Wave Height Using Measured and Computed Minikin Values

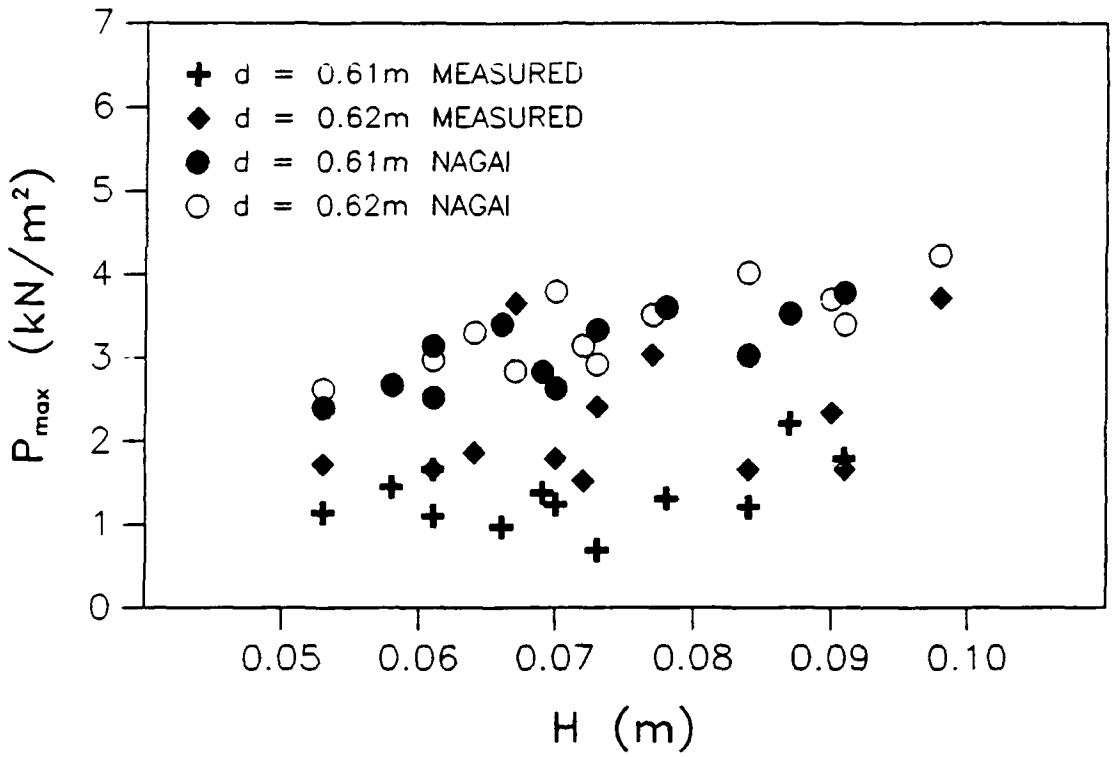

FIG. 13.- Maximum Shock Pressure Versus Wave Height Using Measured and Computed Nagai Values

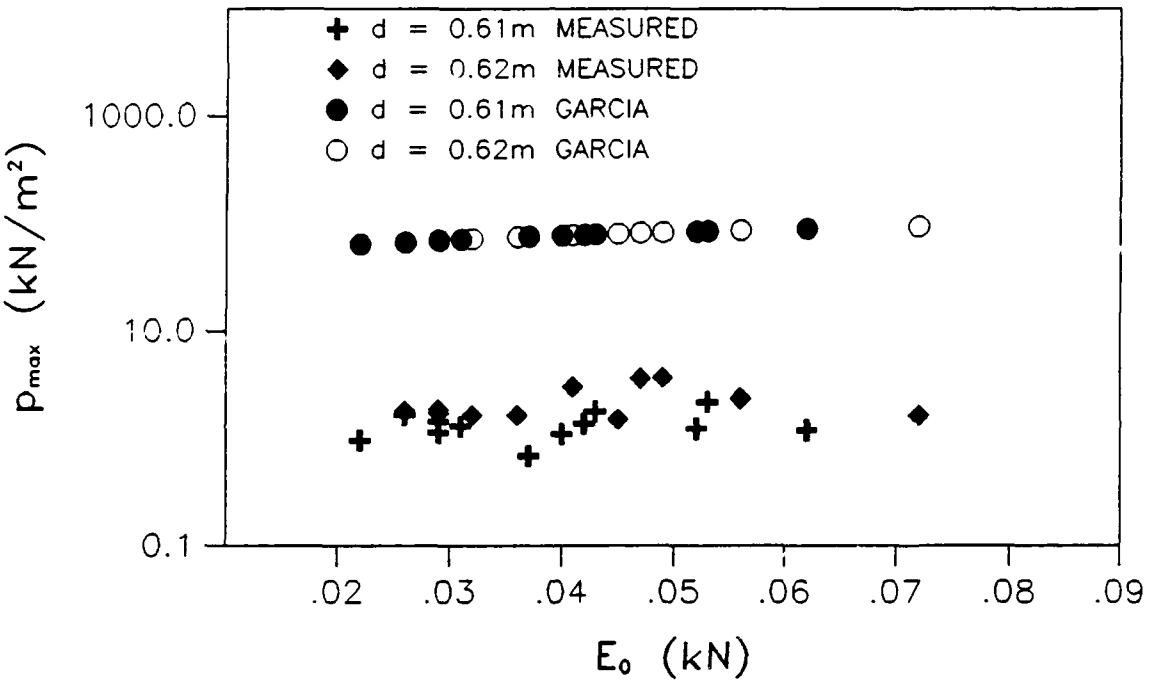

FIG. 14.- Maximum Shock Pressure Versus Deepwater Wave Energy Using Measured and Computed Garcia Values

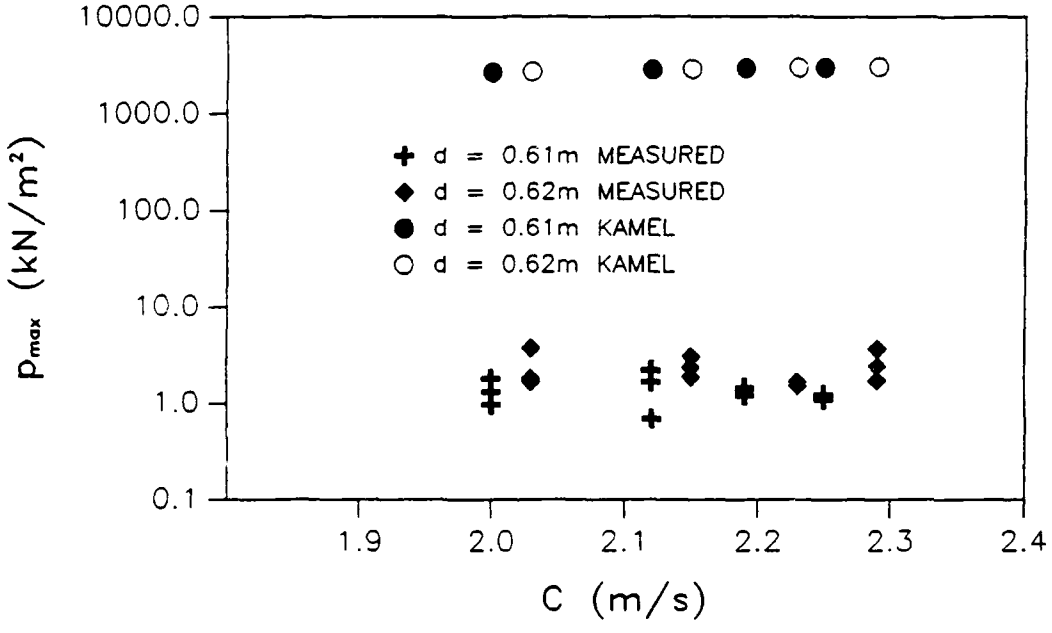

FIG. 15.- Maximum Shock Pressure Versus Wave Celerity Using Measured and Computed Kamel Values

Wave Form and Dynamic Pressure Distribution

Fig. 16 shows a photographic sequence of a wave breaking on the test wall. As can be seen, there is a pocket of air under the crest of the wave before the wave impacts the wall. The measured values in Table 3 verify the fact that the air entrapped between the wave and the wall, decreases the shock pressure. Also, the curvature of the wall causes the entrapped air layer to elongate, increasing its contact surface area. This results in less shock pressure for a recurved wall than a vertical wall. Fig. 16 also shows the amount of reflection and spray affecting the next incoming wave. At times, the impact of the next breaking wave was considerably less than the first.

To further examine the maximum shock pressure, various design curves were generated. The dimensionless maximum shock pressure, $\frac{p_{max}}{p_o}$, was plotted against the parameters of the dimensional analysis results from Chapter IV. These design curves are shown in Figures 17-21. For all curves, data points are plotted for depths equal to 0.61m and 0.62m. The values for the dimensionless parameters from each series are listed in Table I-4. Each curve type is a linear least squares best fit curve. The equation of each line is presented in Table 4.

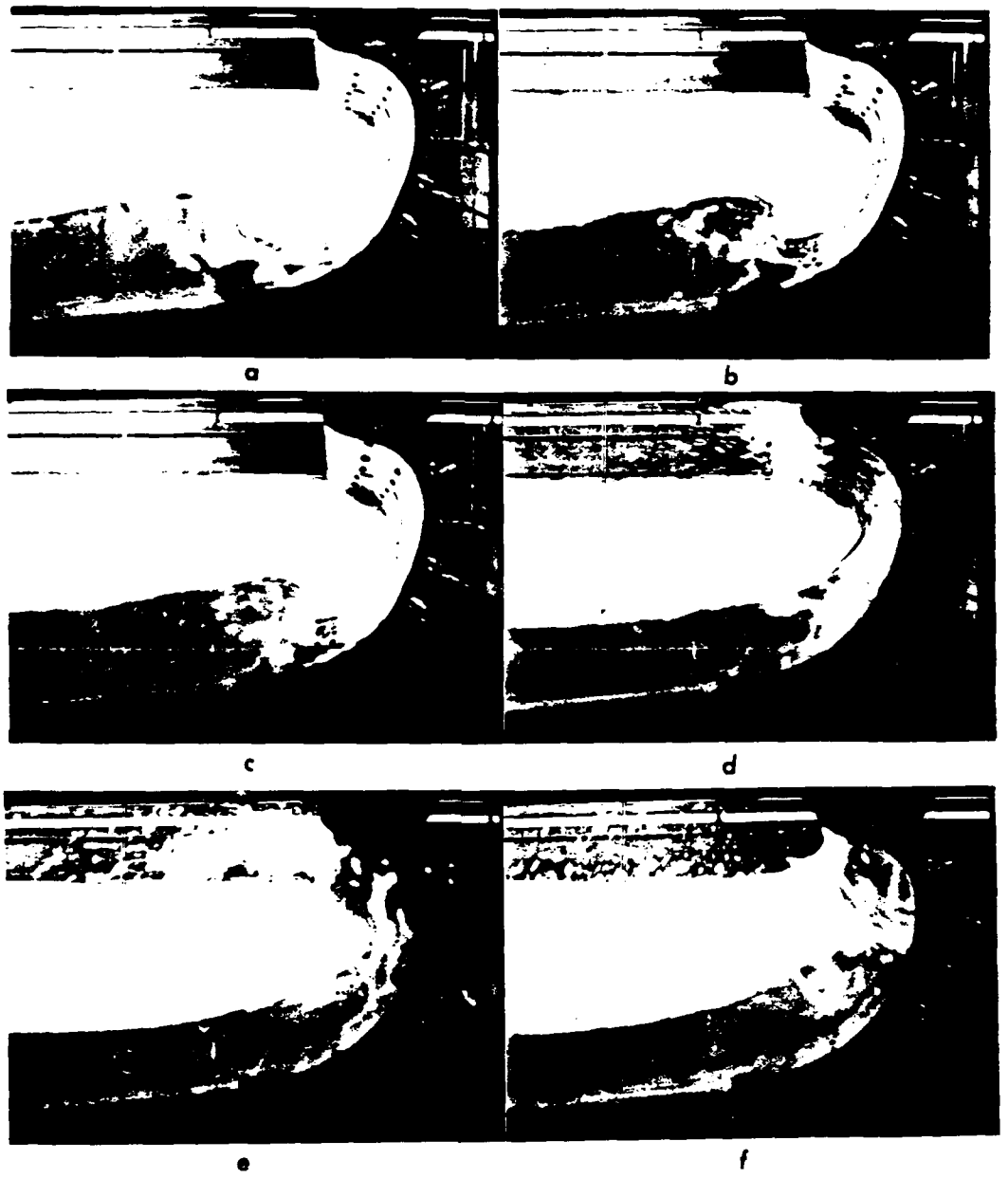

FIG. 16.- Sequence of Breaking Wave on Test Wall

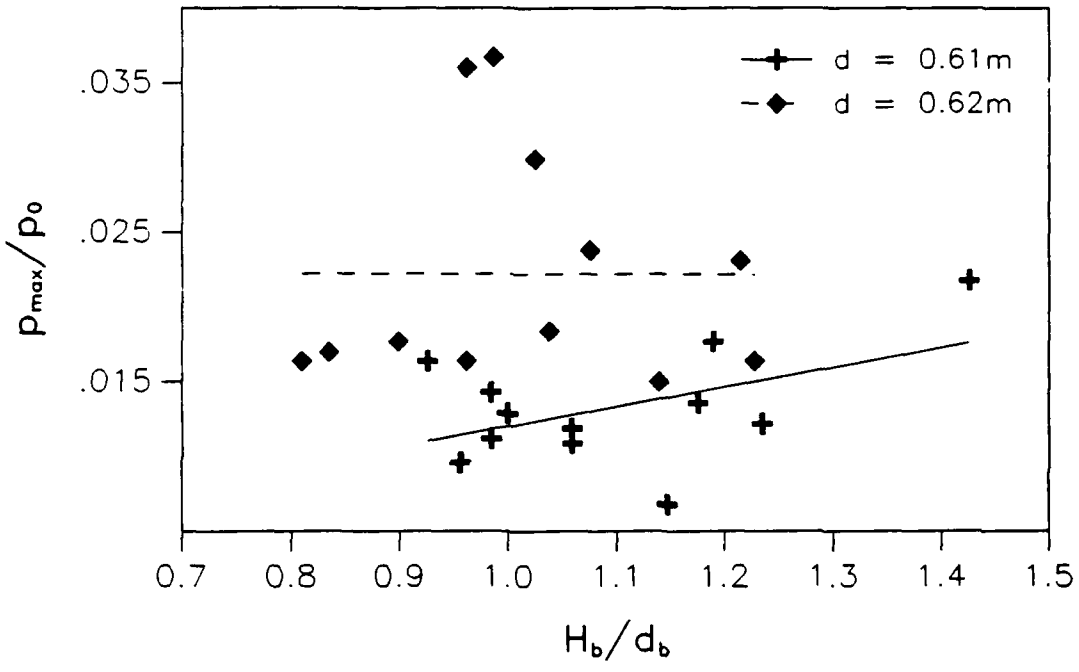

FIG. 17.- Relation Between $\frac{p_{max}}{p_o}$ and $\frac{H_b}{d_b}$

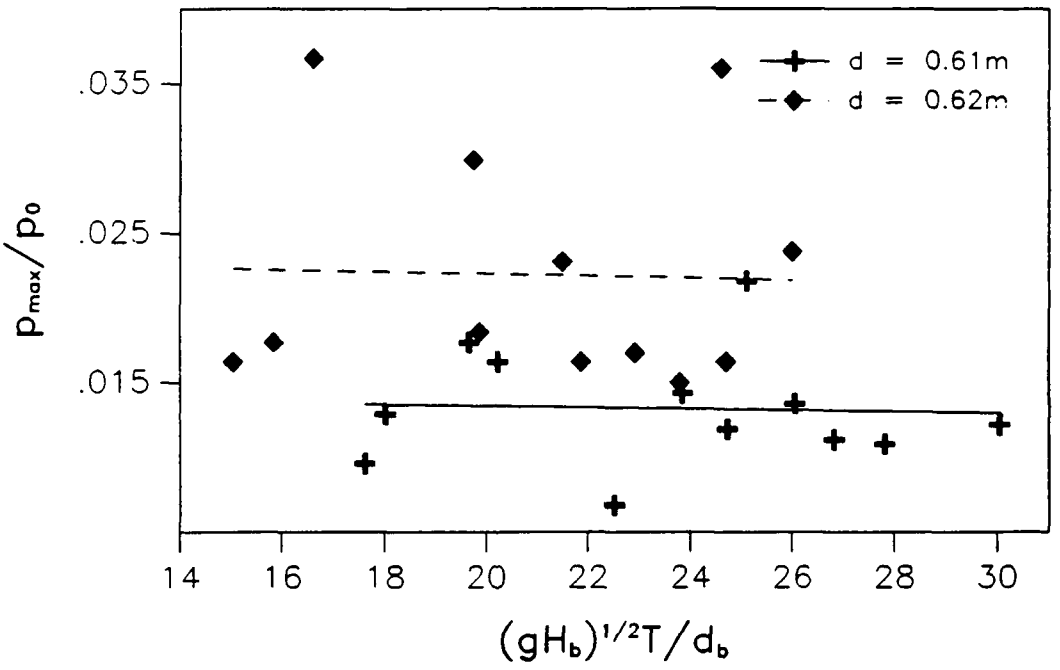

FIG. 18.- Relation Between $\frac{p_{max}}{p_o}$ and $\frac{(gH_b)^{1/2}T}{d_b}$

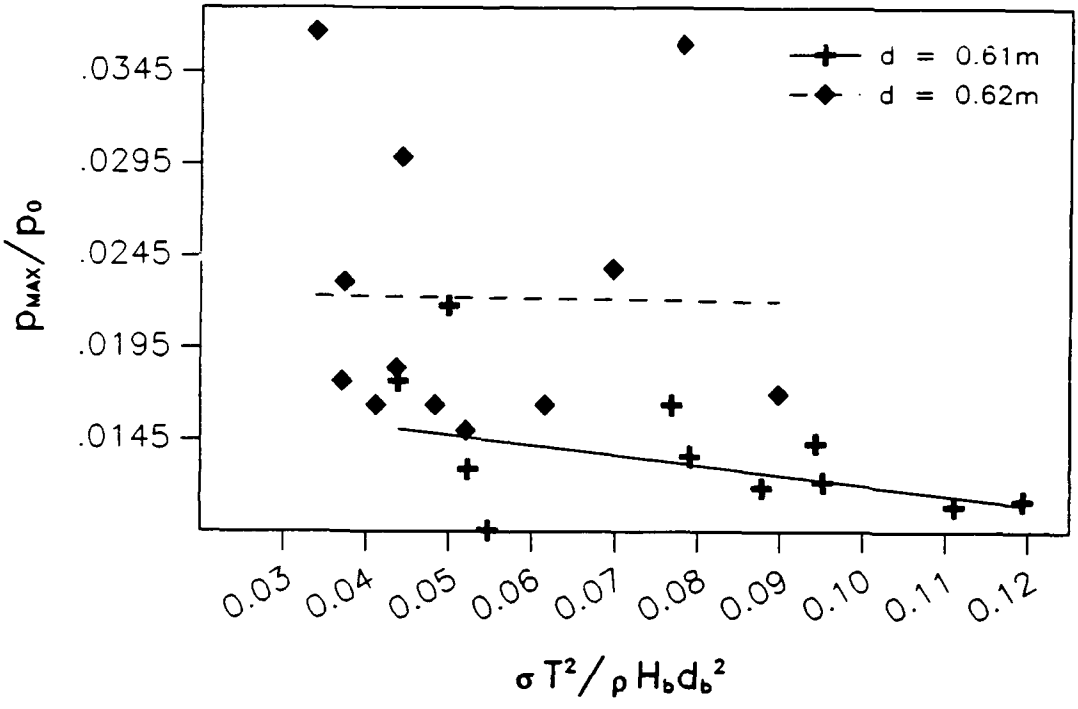

FIG. 19.- Relation Between $\frac{p_{max}}{p_o}$ and $\frac{\sigma T^2}{\rho H_b d_b^2}$

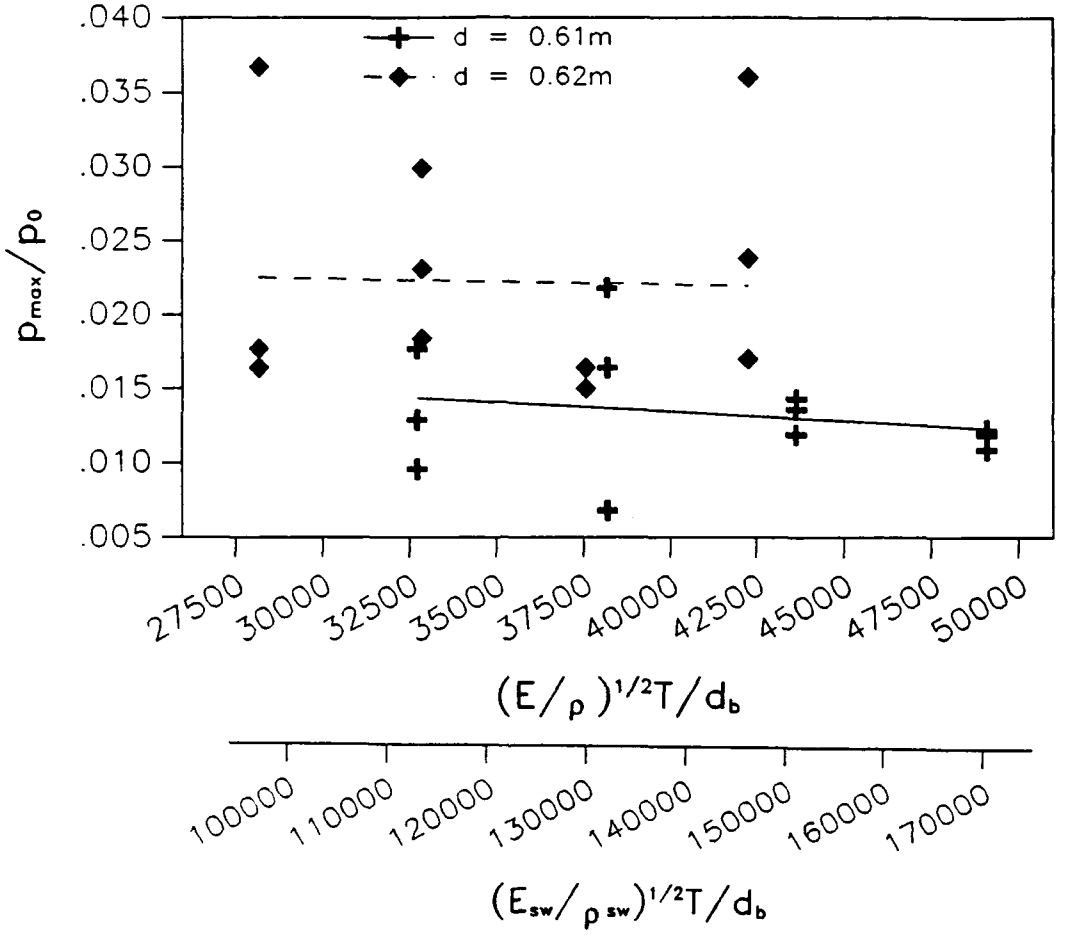

FIG. 20.- Relation Between $\frac{p_{max}}{p_o}$ and $\left(\frac{E}{\rho}\right)^{1/2}\frac{T}{d_b}$, and $\left(\frac{E_{sw}}{\rho_{sw}}\right)^{1/2}\frac{T}{d_b}$

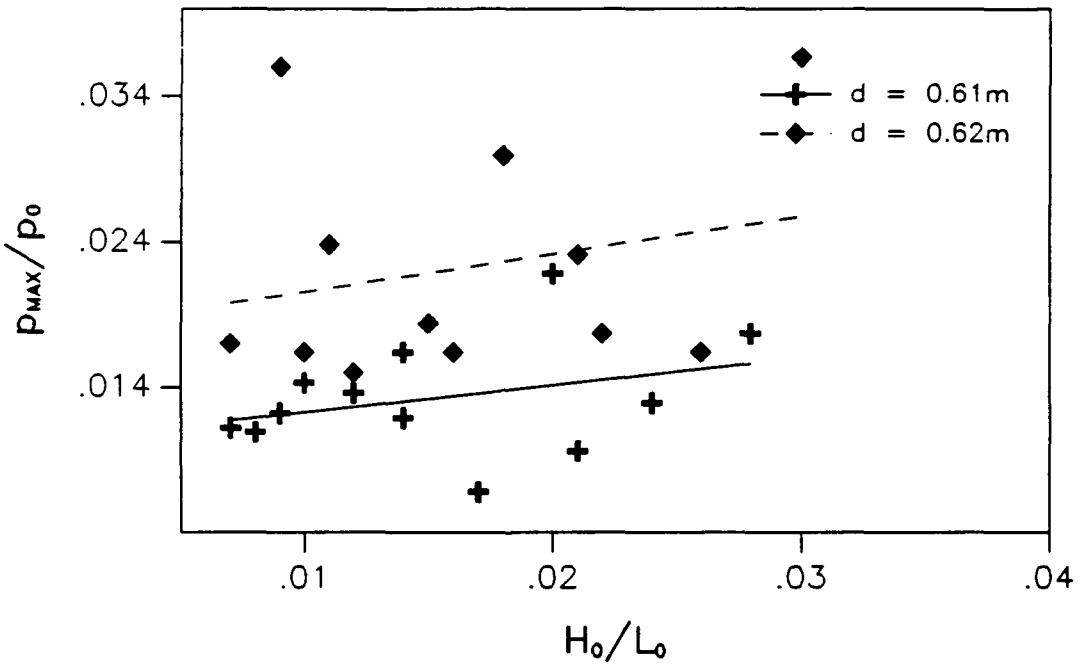

FIG. 21.- Relation Between $\frac{p_{max}}{p_o}$ and $\frac{H_o}{L_o}$

TABLE 4.- Linear Least Square Equations

Parameters	Equation of Line d=0.61m	r^2	d=0.62m	r^2	Fig
$\frac{p_{max}}{p_o}$ vs $\frac{H_b}{d_b}$	$y = 1.2E^{-3} + 1.3E^{-2}x$	0.23	$y = 2.2E^{-2} - 2.2E^{-4}x$	$0.14E^{-5}$	17
			$y = 1.7E^{-2} + 3.8^{E-3}x^*$	$0.6E^{-2}$	
$\frac{p_{max}}{p_o}$ vs $\frac{(gH_b)^{1/2}T}{d_b}$	$y = 1.4E^{-2} - 4.6E^{-5}x$	$0.22E^{-2}$	$y = 2.4E^{-2} - 6.6E^{-5}x$	$0.95E^{-3}$	18
$\frac{p_{max}}{p_o}$ vs $\frac{\sigma T^2}{\rho H_b d_b^2}$	$y = 1.7E^{-2} - 5.5E^{-2}x$	0.12	$y = 2.3E^{-2} - 5.5E^{-3}x$	$0.16E^{-3}$	19
			$y = 2.8E^{-2} - 1.4E^{-2}x^*$	0.12	

TABLE 4.- Continued

Parameters	Equation of Line d=0.61m	r^2	d=0.62m	r^2	Fig
$\frac{p_{max}}{p_o}$ vs $\left(\frac{E}{\rho}\right)^{1/2}\frac{T}{d_b}$	$y = 1.9E^{-2} - 1.4E^{-7}x$	0.05	$y = 2.4E^{-2} - 4.0E^{-8}x$	$0.77E^{-2}$	20
$\frac{p_{max}}{p_o}$ vs $\left(\frac{E_{sw}}{\rho_{sw}}\right)^{1/2}\frac{T}{d_b}$	$y = 1.9E^{-2} - 4.0E^{-8}x$	0.05	$y = 2.4E^{-2} - 1.2E^{-8}x$	$0.77E^{-2}$	20
$\frac{p_{max}}{p_o}$ vs $\frac{H_o}{L_o}$	$y = 1.0E^{-2} + 1.9E^{-1}x$	0.10	$y = 1.8E^{-2} + 2.6E^{-1}x$	0.06	21

*Equation of the line computed without Series 23

Reviewing Figures 17-21, and Table 4, it is difficult to see a linear relation except for Fig. 17 at d=0.61m. All the data points are very scattered, and the correlation coefficients are low. There does seem to be a relationship between $\frac{p_{max}}{p_o}$ and $\frac{H_b}{d_b}$ for d=0.61m in Fig. 17. It appears that as the wave characteristic H_b increases, so does the shock pressure. As previously seen in Figures 12-15, there appeared to be a relationship between the maximum shock pressure and breaking height, incident wave height, and water depth. The measured data points are so scattered, it is hard to see the same trends in Figures 18-21. An example is the measured value from Series 23 in which there is a very large shock pressure for a relatively small wave height, breaking height, and wave steepness (Table I-4). This reinforces the anomaly of the impact phenomona. Without the values of Series 23, the slopes of the linear least squares lines going through the data for both water depths are similar (Table 4).

From the dimensionless curves, there seems to be a relation between maximum shock pressure and water depth. When the water depth increased from 0.61m to 0.62m, the mean maximum shock pressure for water depth increased from 1344.58 N/m^2 to 2252.33 N/m^2.

As presented in Figures 19 and 20, it appears that maximum shock pressure is inversely related to wave period, T. The data points

are very scattered, and to determine the exact relation, additional data may be required.

Fig. 21 represents the relation between dimensionless maximum shock pressure, $\frac{p_{max}}{p_o}$ and deepwater wave steepness, $\frac{H_o}{L_o}$. The plot shows a linear relation, contrary to the Weggel and Maxwell (24) experiments on a vertical wall, in which maximum shock pressure increases with increasing wave steepness. A definite relationship is questionable, again due to the low correlation coefficient shown in Table 4.

Appendix II presents plots of the shock pressure distribution for each series. The mean shock pressure and the peak shock pressure at each transducer are shown. Except for Series 1 and 8, the location of the maximum shock pressure was at Transducer 1. This was due to the limited wave heights produced. The pressure distributions show that maximum pressures at different wall elevations rarely occur simultaneously. This is due to the curvature of the wall. Almost all waves impacted near Transducer 1. It is believed that as wave height increases, the location of maximum pressure will move toward the apex of the small curve of the wall. Also, from these plots, it is seen that the magnitude of the top three transducers increase as the depth increases.

CHAPTER VIII

CONCLUSIONS

The impact of a breaking wave on a seawall causes an initial shock pressure of large magnitude and short duration immediately followed by a secondary pressure of lesser magnitude and longer duration. This study has presented an analysis of the dynamic pressures on a recurved seawall caused by breaking waves. On the basis of the theoretical and experimental considerations, it is concluded that:

1. The magnitude of the shock and secondary pressures are very dependent on the wave characteristics of wave height, H, breaking wave height, H_b, and water depth, d. As the wave height and breaking wave height increase, the magnitude of the shock and secondary pressure increases. A small change in water depth of 0.01m caused a mean pressure increase of approximately 0.09 kN/m^2. Also, it was found that dimensionless maximum shock pressure, $\frac{p_{max}}{p_o}$ is proportional to the deepwater wave steepness, $\frac{H_o}{L_o}$. Due to the curvature of the wall, a layer of air is more readily entrapped causing the magnitude of the shock pressure to decrease. Shock pressures as great as 3.72 kN/m^2 were recorded. The shock pressures measured for apparently identical waves were extremely variable.

2. Maximum shock pressures consistently occurred at the lowest transducer, located closest to the SWL. Although it may not be the precise location of the maximum shock pressure, it was closest to the maximum shock pressure location according to the experimental results. The location of the maximum dynamic pressure on a recurved wall is dependent on the size of the breaking wave, and the curvature of the wall. As the breaking height increases, the location of maximum pressure shifts towards the vertex of the small curvature of the wall.

3. By comparison with vertical wall formulas, the magnitude of the shock pressures on a recurved wall are less than those experienced on a vertical wall. Minikin's formula came closest in agreement to the measured shock pressures, though for design purposes Minikin's formula should be used with care. Other formulas are conservative. In general, the Minikin values were approximately one order of magnitude higher than the measured values, however, for Series 15, 17, and 22-24, the measured values were higher. The other formulas predicted values on the order of 4-100 times greater than the measured values.

4. The secondary pressures on the upper three transducers consistently showed a negative pressure. The largest value being -1.2 kN/m^2. It is concluded that as the wave surge rushes past these transducers on the recurved wall, a suction is formed producing a negative pressure.

5. The magnitude of the maximum shock pressure is very irregular. This is due to the wave form and the amount of air entrapped between the wave and the wall at impact. The wave form that causes the maximum shock pressure is one that has a relativeley large breaking height and steepness, but does not entrap a large quantity of air.

Recommendations for Further Research

There is further research to be accomplished in the area of dynamic pressure on recurved seawalls. Experiments should be done on more than one recurved wall design, with greater wave heights in many different water depths. The pressure distribution can be better described using miniature transducers with a range of 0-25 psia (0-172 kN/m^2) for better resolution, and the number of transducers increased to cover more of the test wall face. The transducers and the test equipment should also be more compatible.

REFERENCES

1. Bagnold, R. A., "Interim Report on Wave Pressure Research." *Journal of the Institution of Civil Engineers*, No 12, London, 1939, pp. 202-226.

2. Berkeley Thorn, R., and Roberts, A. G., *Sea Defense and Coast Protection Works*, Thomas Telford Ltd., London, 1981, pp. 115-121, 179-183.

3. Carr, J. H., "Breaking Wave Forces on Plane Barriers," *Report No. E-11.3*, California Institute of Technology, Pasadena, Cal., Nov 1954, pp. 3-22.

4. Duggal, A., "FAST_SCAN," Unpublished Computer Program, Ocean Engineering Program, Civil Engineering Department, Texas A&M University, 1989.

5. Garcia, W. J., "An Experimental Study of Breaking-Wave Pressures," *Research Report H-68-1*, U.S. Army Engineer Waterways Experiment Station, Vicksburg, Miss., 1968, pp. 3-57.

6. Gouda, M., "Hydrodynamic Wave Pressure on Breakwaters," *Journal of the Waterways, Harbors Division*, ASCE, WW1, March, 1960, pp. 13-25.

7. Grace, P., and Carver, R., "Seawall and Revetment Stability Study, Cape Hatteras Lighthouse, N. C.," *Technical Report CERC-85-12*, U.S. Army Waterways Experiment Station, Coastal Engineering Research Center, Vicksburg, Miss., 1985, pp. 12-39.

8. Heimbaugh, M. S., Grace, P. J., Ahrens, J. P., and Davidson, D. D., "Coastal Engineering Studies in Support of Virginia Beach, Virginia, Beach Erosion Control and Hurricane Protection Project, Report 1, Physical Models Tests of Irregular Wave Overtopping and Pressure Measurements," *Technical Report CERC-88-1*, U.S. Army Waterways Experiment Station, Coastal Engineering Research Center, Vicksburg, Miss., 1988, pp. 6-30.

9. Hudson, R. Y., Hermann, F. A., Jr., Sager, R. A., Whalin, R. W., Keulegan, G. H., Chatham, C. E., Jr., and Hales, L. Z., "Coastal Hydraulic Models," *Special Report No. 5*, U.S. Army Waterways Experiment Station, Coastal Engineering Research Center, Vicksburg, Miss., May, 1979, pp. 320-326.

10. Kamel, A., "Water Wave Pressures on Seawalls and Breakwaters," *Research Report No. 2-10*, U.S. Army Engineer Waterways Experiment Station, Vicksburg, Miss., Feb., 1968, pp. 19-36.

11. Kamel, A., "Shock Pressure on Coastal Structures," *Journal of the Waterways, Harbors and Coastal Engineering Division*, ASCE, Vol. 96, WW3, Aug., 1970, pp. 689-699.

12. Kirkgoz, M. S., "Shock Pressure of Breaking Waves on Vertical Walls," *Journal of the Waterway, Port, Coastal, and Ocean Division*, ASCE, Vol. 108, WW1, Feb., 1982, pp. 81-95.

13. Krafft, M., "MULTI_CAL," Unpublished Computer Program, Ocean Engineering Program, Civil Engineering Department, Texas A&M University, 1989.

14. Krafft, M., "MULTI_SCAN," Unpublished Computer Program, Ocean Engineering Program, Civil Engineering Department, Texas A&M University, 1989.

15. Minikin, R. R., *Winds, Waves, and Maritime Structures*, Griffin, London, 1950, pp. 28-48.

16. Mitsuyasu, H., " Shock Pressure of Breaking Wave," *Proceedings of the 12th Conference of Coastal Engineering*, ASCE, Vol. I, 1966, pp. 268-283.

17. Nagai, S., "Shock Pressures Exerted by Breaking Waves on Breakwaters," *Journal of the Waterways and Harbors Division*, ASCE, WW2, June, 1960, pp. 1-38.

18. Owen, M. W., "The Hydraulic Design of Seawall Profiles," *Shoreline Protection*, London, 1983, pp. 185-192.

19. Richert, G., "Experimental Investigations of Shock Pressures Against Breakwater," *Proceedings of the 11th Conference of Coastal Engineering*, ASCE, Vol. I, 1968, pp 954-973.

20. Ross, C. W., " Shock Pressures of Breaking Waves," *Proceedings of the 4th Conference of Coastal Engineering*, ASCE, Chap. 23, 1953, pp. 323-332.

21. Ross, C. W., "Laboratory Study of Shock Pressures of Breaking Waves," *Technical Manual No. 59*, Beach Erosion Board, U.S. Army, 1955, pp. 6-22.

22. Rundgren, L., "Water Wave Forces; A Theoretical and Laboratory Study," Transactions, Royal Institute of Technology, Institution of Hydraulics, *Bulletin No. 54*, 1958, pp. 84-114.

23. U.S. Army Coastal Engineering Research Center, *Shore Protection Manual*, U.S. Government Printing Office, Washington, D.C., 1984, pp. 2.6-2.8, 7.180-7.200.

24. Weggel, J. R., and Maxwell, W. H., "Experimental Study of Breaking Wave Pressures," *Procedings of the 2nd Offshore Technology Conference, Preprints*, OTC- Paper 1244, Vol. 2, Dallas, Tex., 1970, pp. 175-188.

APPENDICES

APPENDIX I

DATA

TABLE I-1.- Summary Of Wave Data

Test Series	T (sec)	d (m)	d_w (m)	L (m)	L_o (m)	C (m/s)	H (m)	H_b (m)	H_o (m)	pmax (N/m^2)
1	1.50	0.61	0.044	3.01	3.51	2.00	0.066	0.065	0.072	965.0
2	1.50	0.61	0.044	3.01	3.51	2.00	0.078	0.068	0.085	1310.0
3	1.50	0.61	0.044	3.01	3.51	2.00	0.091	0.081	0.100	1793.0
4	1.75	0.61	0.044	3.71	4.78	2.12	0.061	0.063	0.066	1655.0
5	1.75	0.61	0.044	3.71	4.78	2.12	0.073	0.078	0.080	690.0
6	1.75	0.61	0.044	3.71	4.78	2.12	0.087	0.097	0.095	2206.0
7	2.00	0.61	0.044	4.39	6.25	2.19	0.058	0.067	0.062	1448.0
8	2.00	0.61	0.044	4.39	6.25	2.19	0.069	0.080	0.074	1379.0
9	2.00	0.61	0.044	4.39	6.25	2.19	0.084	0.072	0.090	1207.0
10	2.25	0.61	0.044	5.06	7.91	2.25	0.053	0.067	0.055	1138.0
11	2.25	0.61	0.044	5.06	7.91	2.25	0.061	0.072	0.064	1103.0
12	2.25	0.61	0.044	5.06	7.91	2.25	0.070	0.084	0.073	1241.0
13	1.50	0.62	0.054	3.04	3.51	2.03	0.070	0.071	0.077	1793.0
14	1.50	0.62	0.054	3.04	3.51	2.03	0.084	0.064	0.092	1655.0

Table I-1.- Continued

Test Series	T (sec)	d (m)	d_w (m)	L (m)	L_o (m)	C (m/s)	H (m)	H_b (m)	H_o (m)	pmax (N/m^2)
15	1.50	0.62	0.054	3.04	3.51	2.03	0.098	0.078	0.107	3723.0
16	1.75	0.62	0.054	3.76	4.78	2.15	0.064	0.082	0.070	1862.0
17	1.75	0.62	0.054	3.76	4.78	2.15	0.077	0.081	0.084	3033.0
18	1.75	0.62	0.054	3.76	4.78	2.15	0.090	0.096	0.098	2344.0
19	2.00	0.62	0.054	4.46	6.25	2.23	0.061	0.076	0.065	1655.0
20	2.00	0.62	0.054	4.46	6.25	2.23	0.072	0.090	0.077	1517.0
21	2.00	0.62	0.054	4.46	6.25	2.23	0.091	0.097	0.097	1655.0
22	2.25	0.62	0.054	5.14	7.91	2.29	0.053	0.066	0.055	1724.0
23	2.25	0.62	0.054	5.14	7.91	2.29	0.067	0.076	0.070	3654.0
24	2.25	0.62	0.054	5.14	7.91	2.29	0.073	0.085	0.076	2413.0

TABLE I-2.- Shock Pressure Data

Shock Pressure (N/m^2)						
Series	Run	Transducer				
		1	2	3	4	5
1	1	690	965	-	414	138
	2	724	552	-	138	-
	3	552	827	138	207	-
2	1	1310	827	276	552	138
	2	1241	1172	276	345	69
	3	1172	827	483	207	69
3	1	1792	690	-	-	-
	2	1172	1034	138	138	207
	3	1103	690	414	138	69
4	1	1655	517	-	69	207
	2	690	414	138	138	138
	3	793	517	138	69	138
5	1	690	552	276	69	138
	2	552	483	207	69	138
	3	690	552	345	138	138
6	1	2206	758	186	207	207
	2	1103	483	207	345	345
	3	1448	552	138	138	414
7	1	827	1000	690	345	69
	2	827	1207	517	621	-
	3	1448	931	483	414	-
8	1	1241	1379	483	414	207
	2	1172	1034	483	345	69
	3	1172	1379	345	276	345
9	1	896	552	138	207	207
	2	1207	552	-	207	345
	3	1103	621	207	276	-

TABLE I-2.- Continued

Series	Run	Shock Pressure (N/m^2) Transducer 1	2	3	4	5
10	1	1138	414	207	414	138
	2	690	345	138	207	69
	3	965	345	414	276	-
11	1	1034	207	207	-	69
	2	1034	379	138	-	138
	3	1103	276	207	-	-
12	1	1241	965	138	483	138
	2	1241	552	758	552	207
	3	1207	414	138	207	138
13	1	1793	1103	310	207	-
	2	1586	1448	69	138	-
	3	1586	655	276	207	-
14	1	1241	1241	827	276	896
	2	1655	1172	690	276	-
	3	1379	1103	621	207	69
15	1	3034	1172	345	1172	207
	2	2482	1172	586	621	138
	3	3723	1379	207	207	138
16	1	1862	1345	345	552	-
	2	1241	1034	345	552	414
	3	1517	1172	345	414	345
17	1	1586	1241	483	345	207
	2	3034	1793	-	345	207
	3	3034	1586	276	690	-

TABLE I-2.- Continued

Series	Run	Shock Pressure (N/m^2) Transducer 1	2	3	4	5
18	1	2344	1241	552	758	345
	2	2344	1103	414	758	138
	3	2275	1034	276	276	207
19	1	1586	758	1034	414	-
	2	1655	896	965	276	207
	3	1655	827	414	-	207
20	1	1517	1103	1103	1241	345
	2	1448	1310	690	1103	207
	3	1448	1172	758	552	414
21	1	1586	1655	345	276	345
	2	1655	1586	621	827	207
	3	1241	1241	414	827	276
22	1	1724	1172	138	-	-
	2	1724	896	345	207	207
	3	1172	1172	-	-	-
23	1	2620	1310	758	138	-
	2	3034	414	483	-	-
	3	3654	896	-	-	-
24	1	2413	896	138	69	207
	2	2069	690	207	138	69
	3	1931	827	138	-	-

TABLE I-3.- Secondary Pressure Data

Series	Run	Secondary Pressure (N/m^2) Transducer 1	2	3	4	5
1	1	552	552	-758	-758	-414
	2	552	207	-758	-552	-690
	3	517	414	-690	-552	-827
2	1	565	345	-827	-827	-1034
	2	552	345	-690	-1034	-1034
	3	552	414	-758	-896	-1034
3	1	655	483	-758	-758	-1034
	2	552	414	-690	-758	-483
	3	552	379	-690	-690	-690
4	1	414	241	-827	-758	-1034
	2	552	345	-965	-758	-621
	3	483	345	-758	-758	-690
5	1	448	400	-896	-862	-621
	2	276	207	-896	-827	-690
	3	414	276	-896	-758	-758
6	1	690	414	-552	-758	-965
	2	690	414	-552	-827	-1034
	3	690	414	-758	-827	-896
7	1	690	345	-690	-965	-965
	2	414	276	-758	-758	-827
	3	483	414	-758	-690	-896
8	1	621	552	-552	-414	-552
	2	552	379	-621	-552	-483
	3	690	621	-724	-621	-690
9	1	690	69	-1034	-896	-1034
	2	690	483	-1034	-1103	-1172
	3	621	207	-1034	-896	-1034

TABLE I-3.- Continued

Series	Run	Secondary Pressure (N/m^2) Transducer 1	2	3	4	5
10	1	621	414	-207	-827	-207
	2	483	276	-621	-552	-414
	3	483	276	-552	-414	-345
11	1	552	207	-690	-758	-758
	2	690	448	-552	-483	-483
	3	552	276	-690	-690	-690
12	1	552	345	-690	-483	-896
	2	621	414	-758	-827	-827
	3	758	276	-896	-1034	-965
13	1	690	552	-827	-621	-896
	2	621	345	-827	-896	-896
	3	621	483	-345	-621	-552
14	1	552	414	-1034	-965	-1103
	2	690	414	-1034	-1034	-1034
	3	690	276	-1034	-827	-1172
15	1	690	345	-690	-1034	-1034
	2	690	345	-827	-621	-1103
	3	827	414	-758	-1034	-1103
16	1	690	483	-827	-690	-896
	2	690	345	-827	-276	-552
	3	690	414	-690	-758	-690
17	1	827	483	-552	-483	-690
	2	827	552	-827	-965	-1172
	3	690	414	-1172	-1103	-1172
18	1	690	483	-896	-1034	-1241
	2	827	414	-896	-1034	-1241
	3	690	345	-965	-1034	-1103

TABLE I-3.- Continued

Series	Run	Secondary Pressure (N/m^2) Transducer 1	2	3	4	5
19	1	690	345	-965	-827	-896
	2	690	207	-1034	-896	-1172
	3	552	345	-1586	-1034	-1103
20	1	758	552	-827	-690	-896
	2	621	345	-827	-758	-758
	3	621	276	-827	-621	-827
21	1	690	414	-690	-758	-827
	2	621	345	-827	-758	-758
	3	690	414	-690	-552	-896
22	1	552	241	-827	-827	-758
	2	552	414	-758	-758	-758
	3	552	345	-896	-758	-690
23	1	690	345	-1172	-1172	-1103
	2	552	207	-1241	-1034	-1241
	3	690	207	-1172	-1034	-1034
24	1	621	276	-1172	-896	-1241
	2	552	207	-1241	-896	-1241
	3	552	276	-1172	-1034	-1241

TABLE I-4.- Dimensionless Parameters

Series	$\frac{p_{max}}{p_o}$	$\frac{H_b}{d_b}$	$\frac{(gH_b)^{1/2}T}{d_b}$	$\frac{gT^2}{\rho H_b d_b^2}$	$\left(\frac{E}{\rho}\right)^{1/2}\frac{T}{d_b}$	$\left(\frac{E_{sw}}{\rho_{sw}}\right)^{1/2}\frac{T}{d_b}$	$\frac{H_o}{L_o}$
1	0.0096	0.9560	17.6150	0.0547	32729.9800	112652.7900	0.0210
2	0.0129	1.0000	18.0170	0.0523	32729.9800	112652.7900	0.0240
3	0.0177	1.1910	19.6630	0.0439	32729.9800	112652.7900	0.0280
4	0.0164	0.9260	20.2320	0.0768	38184.9800	131428.2500	0.0140
5	0.0068	1.1470	22.5120	0.0620	38184.9800	131428.2500	0.0170
6	0.0218	1.4260	25.1040	0.0499	38184.9800	131428.2500	0.0200
7	0.0143	0.9850	23.8450	0.0943	43639.9700	150203.7100	0.0100
8	0.0136	1.1760	26.0560	0.0790	43639.9700	150203.7100	0.0120
9	0.0119	1.0590	24.7180	0.0878	43639.9700	150203.7100	0.0140
10	0.0112	0.9850	26.8250	0.1194	49094.9700	168979.1800	0.0070

TABLE I-4.- Continued

Series	$\frac{p_{max}}{p_o}$	$\frac{H_b}{d_b}$	$\frac{(gH_b)^{1/2}T}{d_b}$	$\frac{\sigma T^2}{\rho H_b d_b^2}$	$\left(\frac{E}{\rho}\right)^{1/2}\frac{T}{d_b}$	$\left(\frac{E_{sw}}{\rho_{sw}}\right)^{1/2}\frac{T}{d_b}$	$\frac{H_o}{L_o}$
11	0.0109	1.0590	27.8080	0.1111	49094.9700	168979.1800	0.0080
12	0.0122	1.2350	30.0360	0.0952	49094.9700	168979.1800	0.0090
13	0.0177	0.8990	15.8460	0.0371	28172.6400	96966.9500	0.0220
14	0.0164	0.8100	15.0450	0.0412	28172.6400	96966.9500	0.0260
15	0.0367	0.9870	16.6090	0.0338	28172.6400	96966.9500	0.0300
16	0.0184	1.0380	19.8680	0.0437	32868.0800	113128.1100	0.0150
17	0.0299	1.0250	19.7460	0.0443	32868.0800	113128.1100	0.0180
18	0.0231	1.2150	21.4970	0.0373	32868.0800	113128.1100	0.0210
19	0.0164	0.9620	21.8600	0.0616	37563.5200	129289.2700	0.0100
20	0.0150	1.1390	23.7880	0.0520	37563.5200	129289.2700	0.0120

TABLE I-4.- Continued

Series	$\frac{p_{max}}{p_o}$	$\frac{H_b}{d_b}$	$\frac{(gH_b)^{1/2}T}{d_b}$	$\frac{gT^2}{\rho H_b d_b^2}$	$\left(\frac{E}{\rho}\right)^{1/2}\frac{T}{d_b}$	$\left(\frac{E_{sw}}{\rho_{sw}}\right)^{1/2}\frac{T}{d_b}$	$\frac{H_o}{L_o}$
21	0.0164	1.2280	24.6960	0.0483	37563.5200	129289.2700	0.0160
22	0.0170	0.8350	22.9170	0.0898	42258.9600	145450.4300	0.0070
23	0.0360	0.9620	24.5920	0.0780	42258.9600	145450.4300	0.0090
24	0.0238	1.0760	26.0080	0.0697	42258.9600	145450.4300	0.0110

APPENDIX II

SHOCK PRESSURE DISTRIBUTION

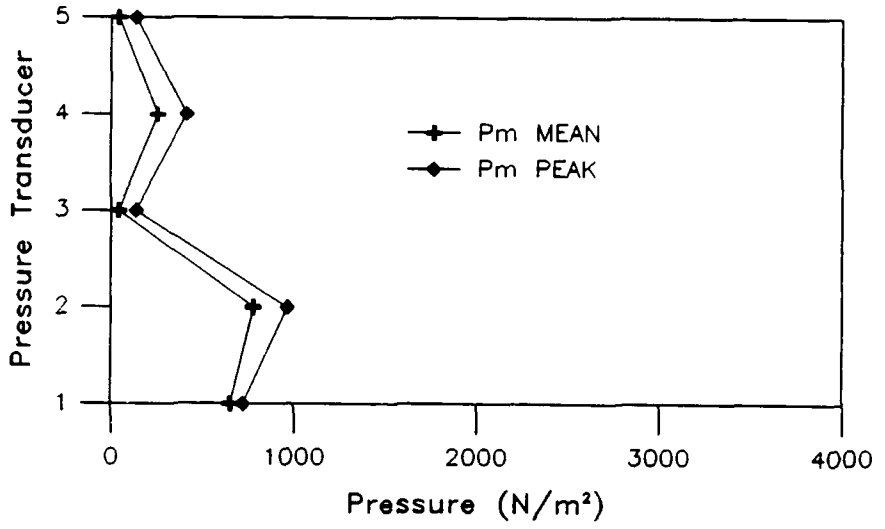

FIG. 22.- Pressure Distribution Series 1

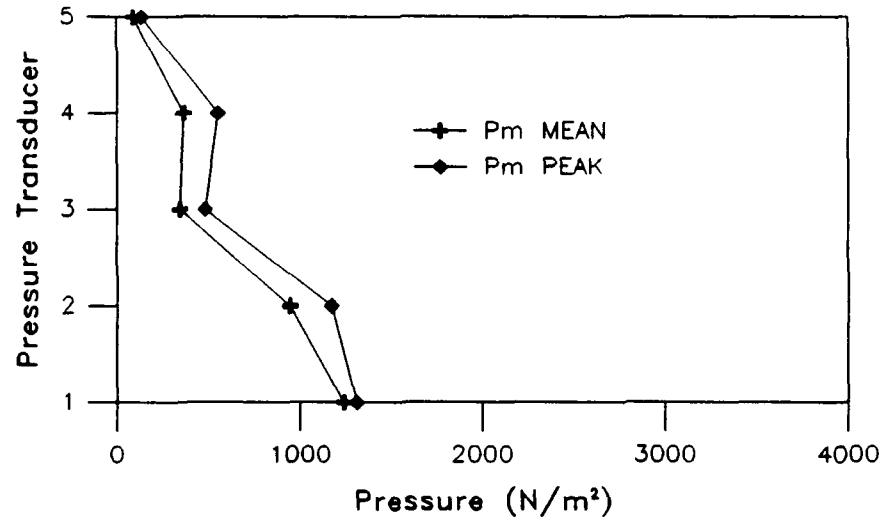

FIG. 23.- Pressure Distribution Series 2

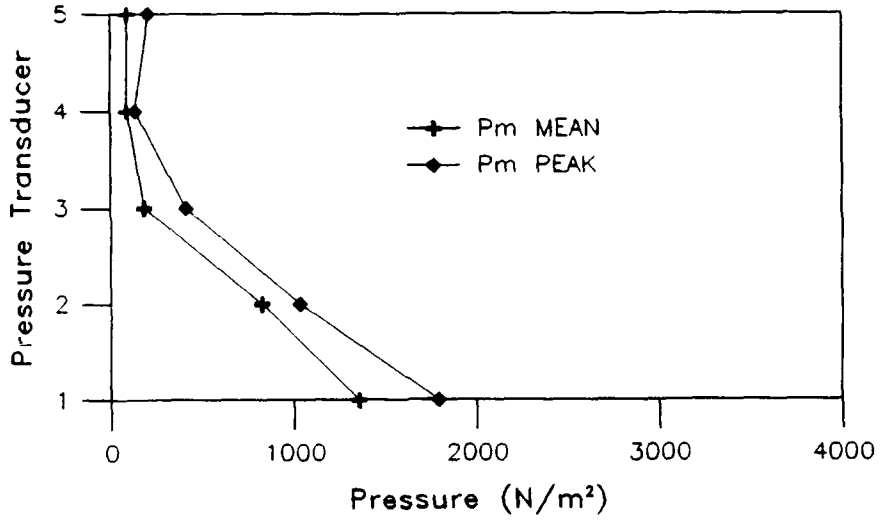

FIG. 24.- Pressure Distribution Series 3

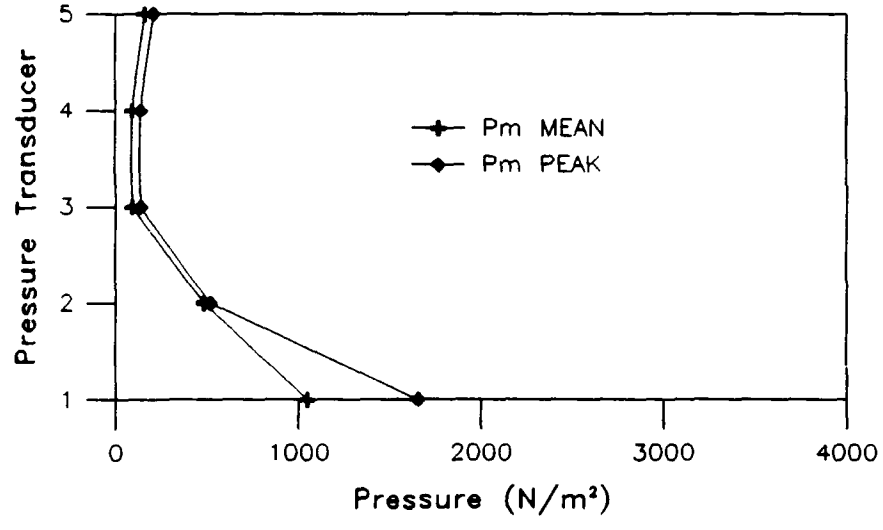

FIG. 25.- Pressure Distribution Series 4

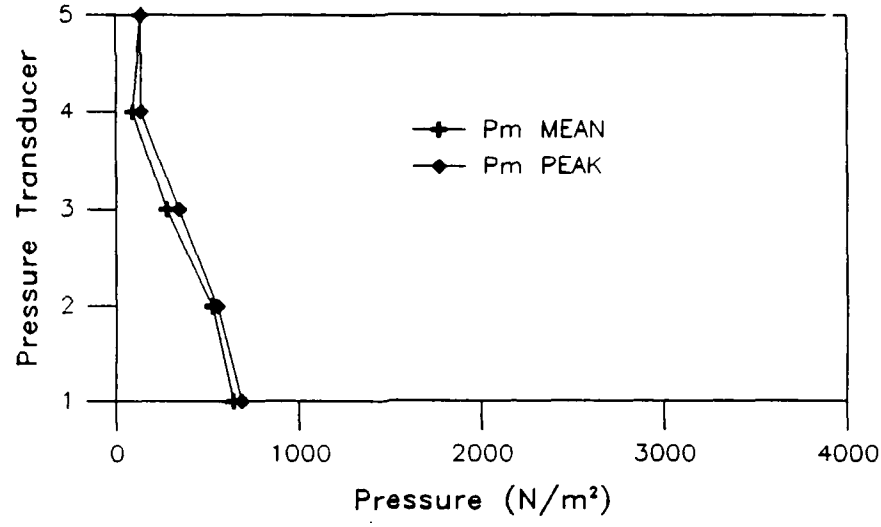

FIG. 26.- Pressure Distribution Series 5

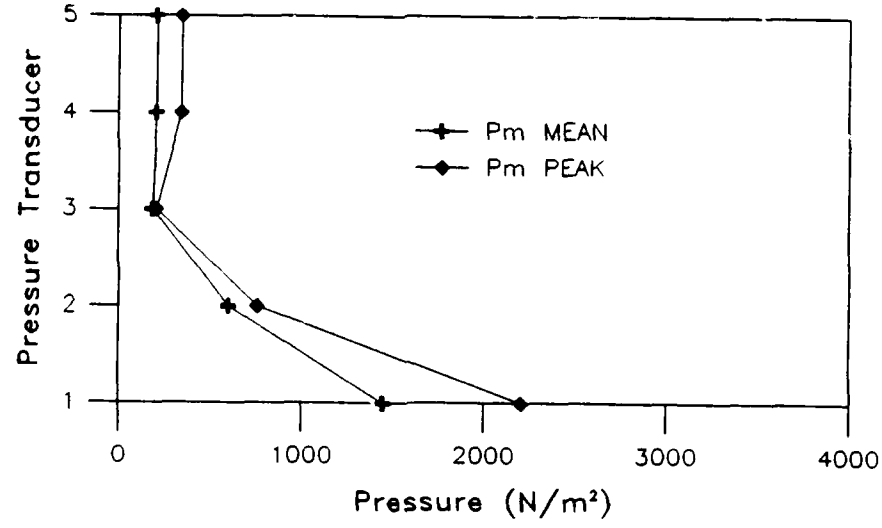

FIG. 27.- Pressure Distribution Series 6

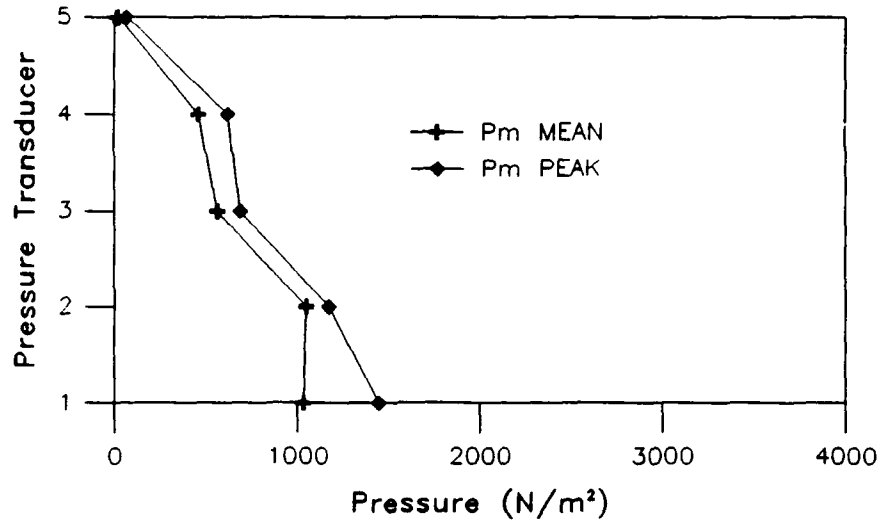

FIG. 28.- Pressure Distribution Series 7

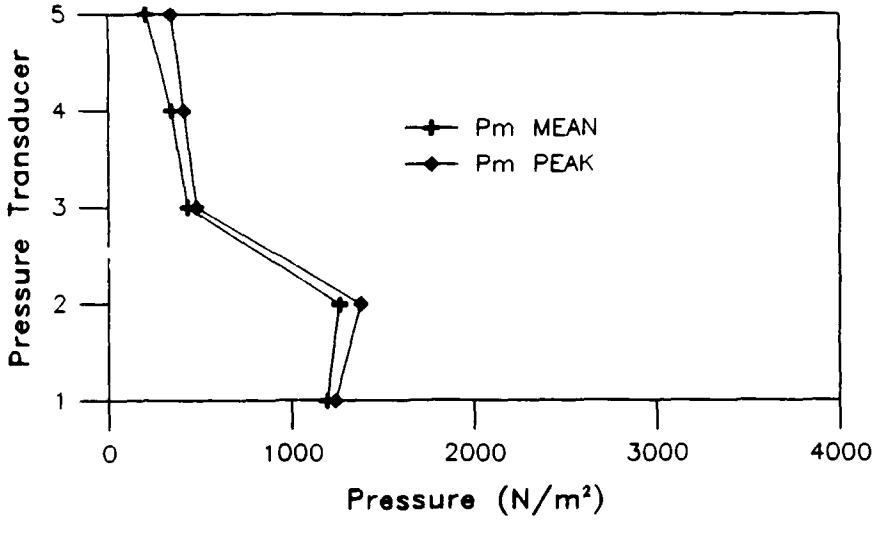

FIG. 29.- Pressure Distribution Series 8

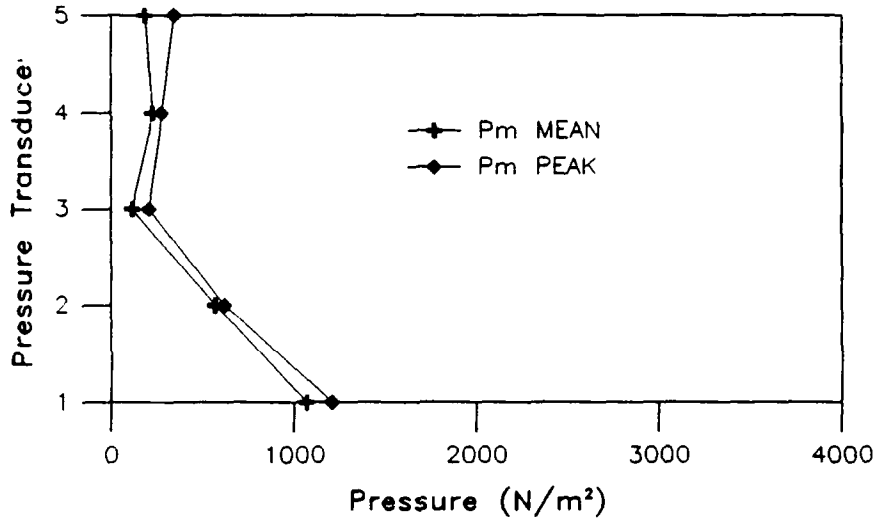

FIG. 30.- Pressure Distribution Series 9

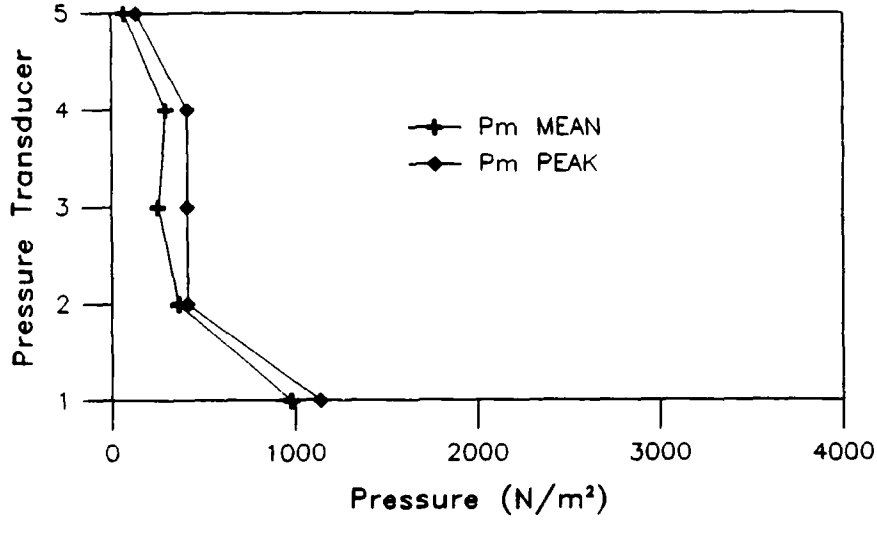

FIG. 31.- Pressure Distribution Series 10

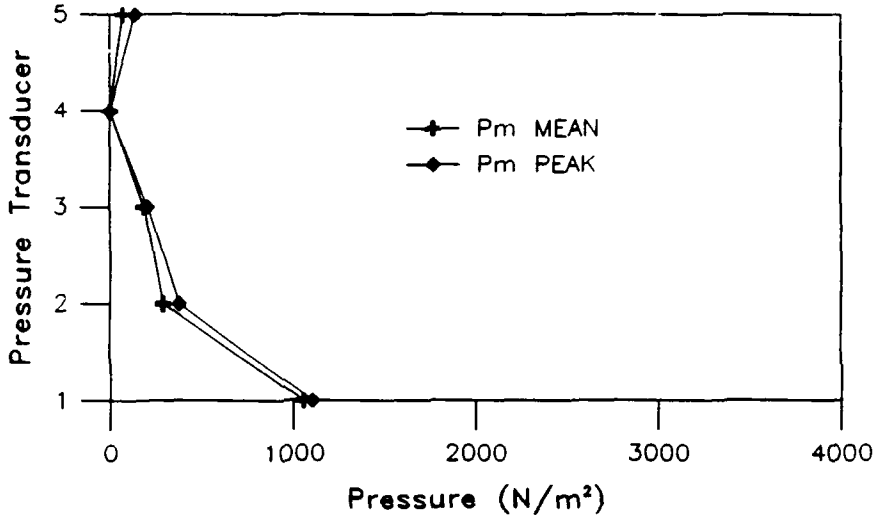

FIG. 32.- Pressure Distribution Series 11

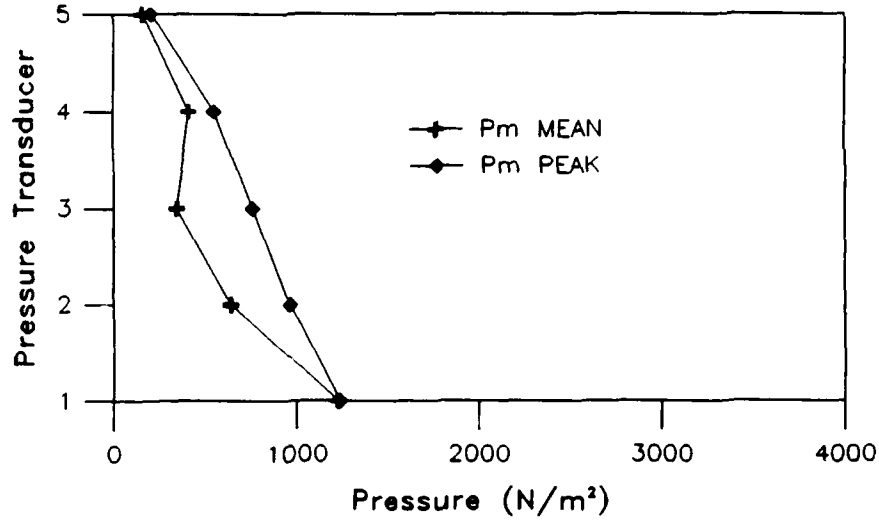

FIG. 33.- Pressure Distribution Series 12

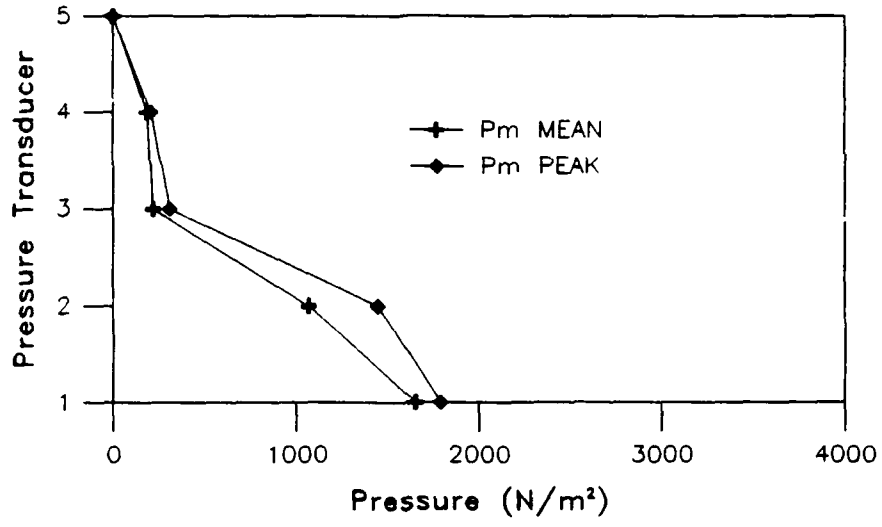

FIG. 34.- Pressure Distribution Series 13

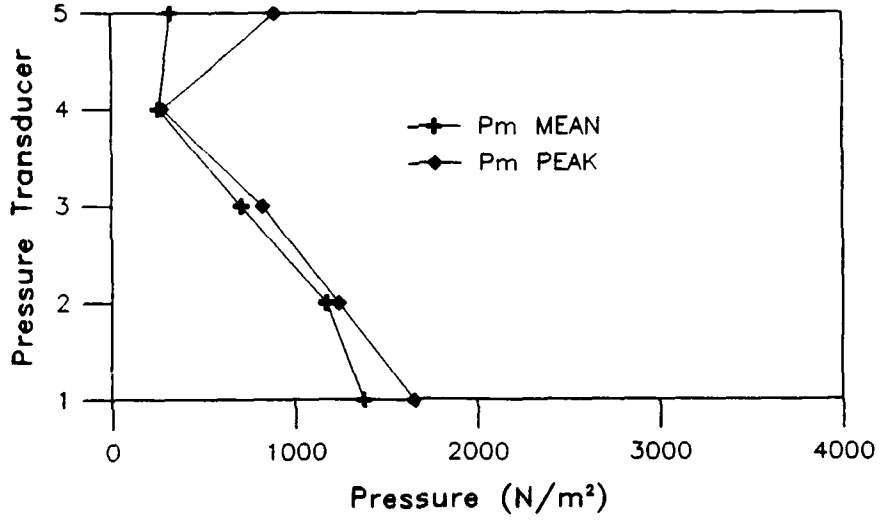

FIG. 35.- Pressure Distribution Series 14

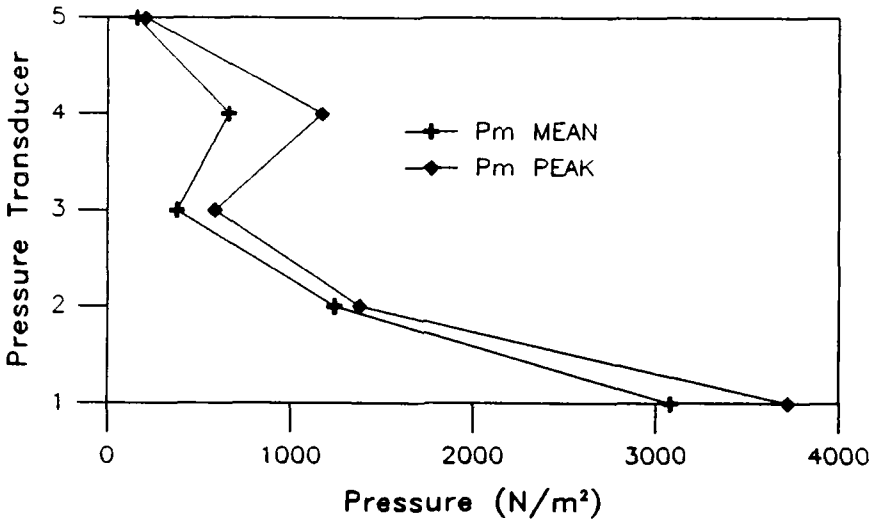

FIG. 36.- Pressure Distribution Series 15

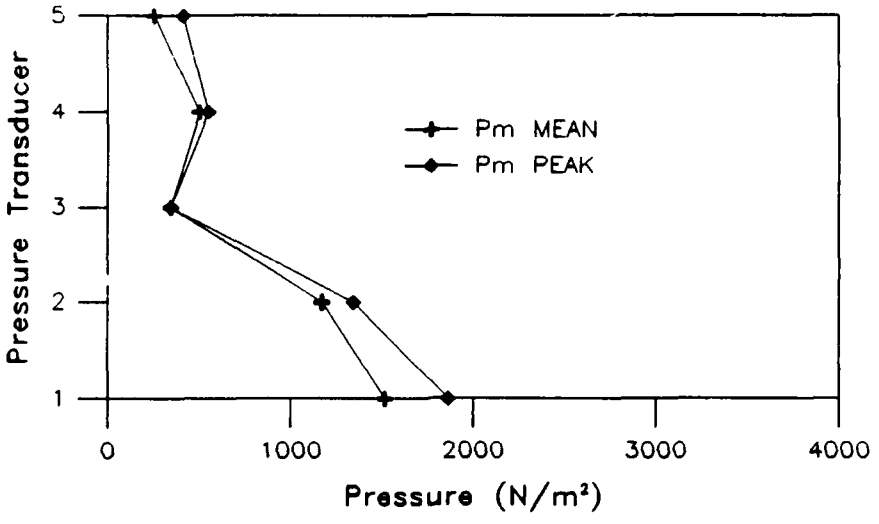

FIG. 37.- Pressure Distribution Series 16

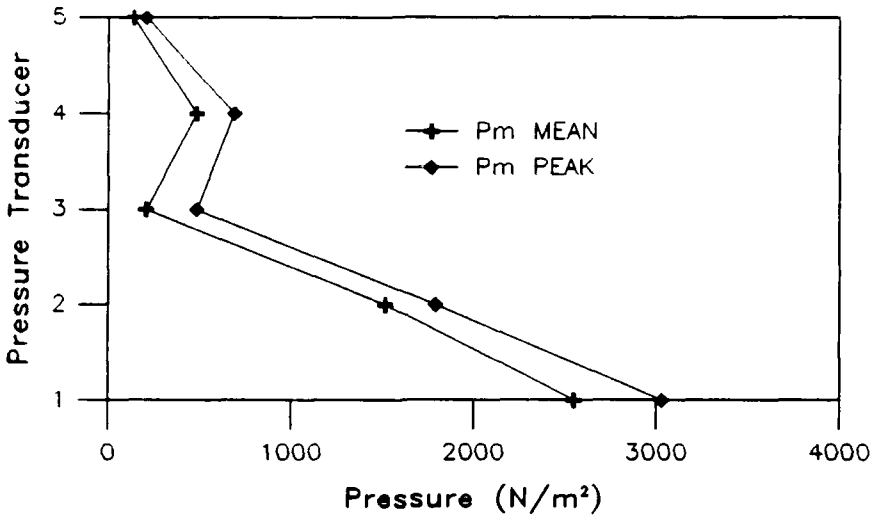

FIG. 38.- Pressure Distribution Series 17

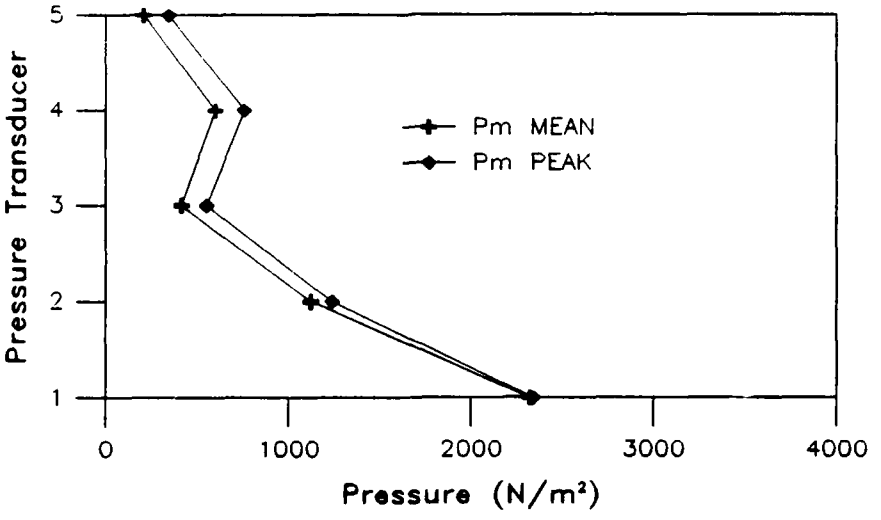

FIG. 39.- Pressure Distribution Series 18

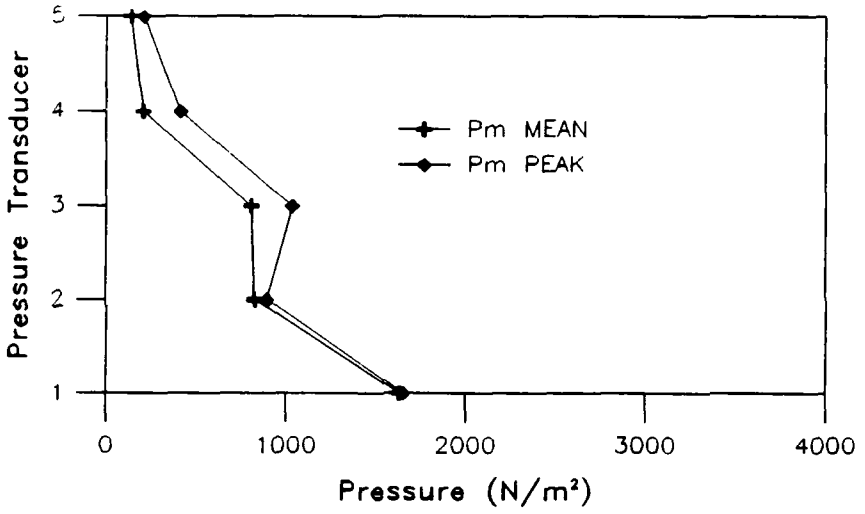

FIG. 40.- Pressure Distribution Series 19

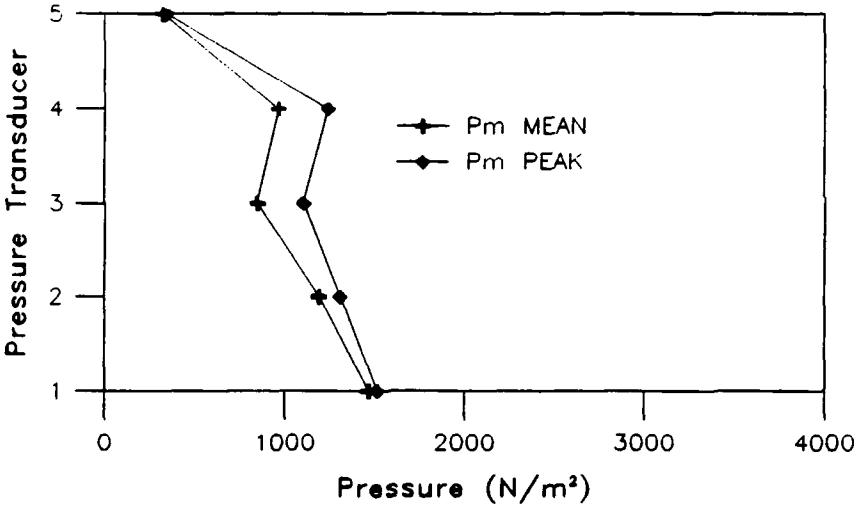

FIG. 41.- Pressure Distribution Series 20

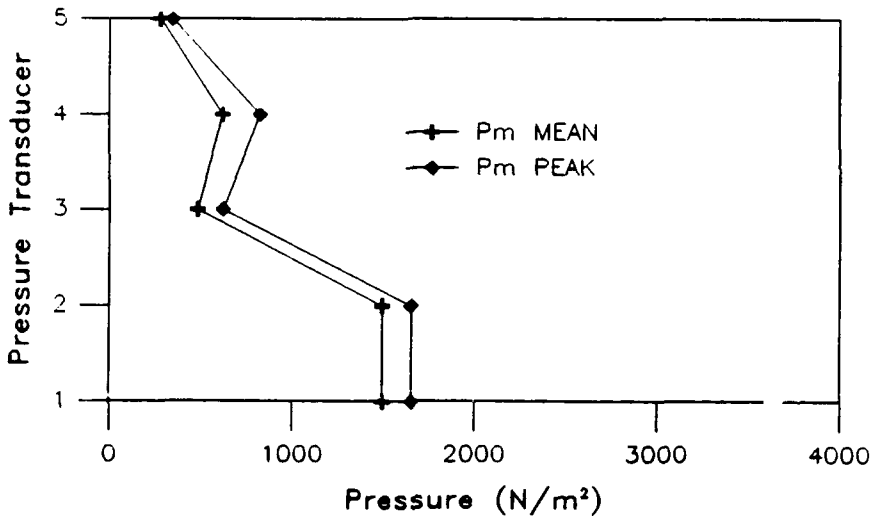

FIG. 42.- Pressure Distribution Series 21

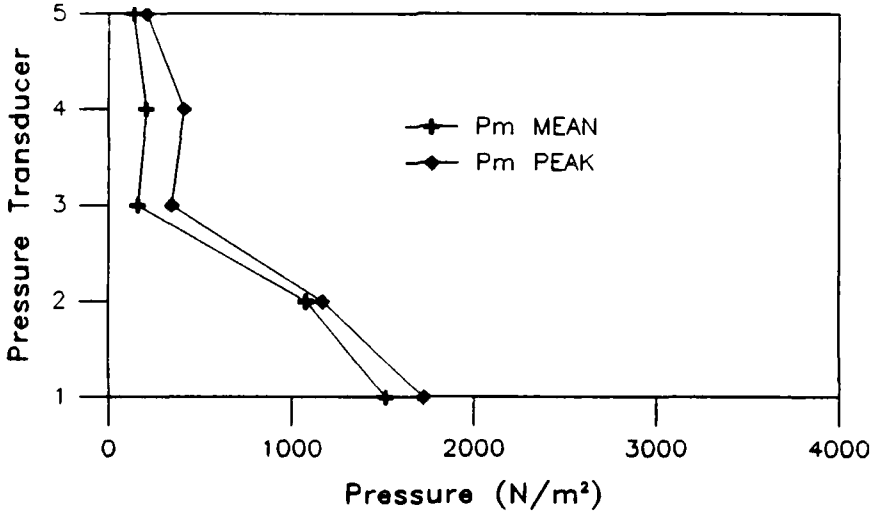

FIG. 43.- Pressure Distribution Series 22

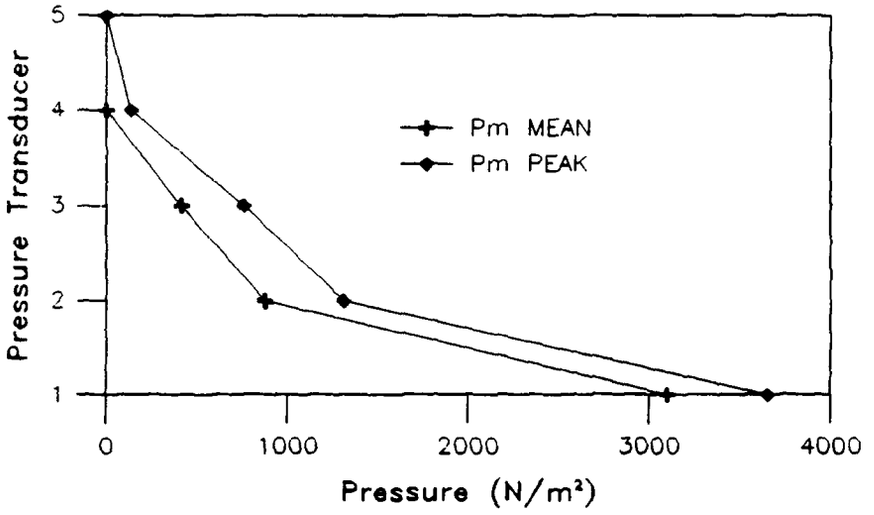

FIG. 44.- Pressure Distribution Series 23

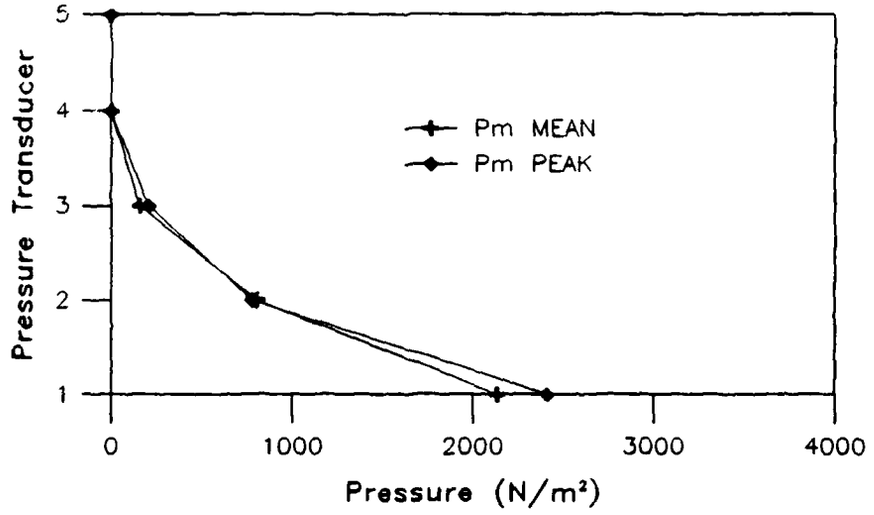

FIg. 45.- Pressure Distribution Series 24

APPENDIX III

NOTATION

The following symbols are used in this paper:

A	= area
C	= wave celerity
C_w	= acoustic velocity in water
C_{sw}	= acoustic velocity in seawall
d	= still water depth
D	= still water depth one wave length seaward of wall
D_T	= thickness of entrapped air layer
d_b	= still water depth at breaking
d_w	= still water depth at the wall
E	= modulus of elasticity of the water
E_o	= deepwater wave energy
E_{sw}	= bulk modulus of the seawall
F	= force acting on mass of fluid
f	= function
g	= acceleration due to gravity
H	= wave height at depth, d
H_b	= wave height at breaking
H_o	= deep water wave height
k	= adiabatic constant of air
ℓ	= length of water mass
L	= wave length at depth, d
L_D	= wave length at depth, D
L_o	= deep water wave length
p	= pressure
p_o	= atmospheric pressure
p_m	= shock pressure
p_{max}	= maximum shock pressure
p_s	= secondary pressure
r^2	= correlation coefficient

SWL	=	still water level
t	=	time
t_m	=	time at p_m
T	=	wave period
u	=	velocity
u_b	=	velocity at breaking
U	=	wind velocity
β	=	angle of incident wave attack
γ	=	weight per unit volume of water
θ	=	angle of bottom slope
ρ	=	mass density of the water
ρ_{sw}	=	mass density of the seawall
σ	=	surface tension of the water

VITA

Gregory Ross Rismiller [redacted] He attended Virginia Polytechnic Institute and State University, earning Bachelor of Science Degrees in Civil Engineering in 1980, and Building Construction in 1981. Upon graduation he was commissioned an Ensign, Civil Engineer Corps, U. S. Navy Reserve, and has remained on active duty since that time.

Since receiving his commission, Mr. Rismiller has served as Maintenance Officer for the Public Works Department, Marine Corps Air Station, Iwakuni, Japan, and as Assistant Company Commander and Elevated Causeway Team Officer in Charge, Amphibious Construction Battalion TWO, Little Creek, Virginia. Just prior to his attendance at Texas A&M University, he was Officer in Charge, Naval Construction Battalion Unit FOUR ONE ONE, Norfolk, Virginia. He now holds the rank of Lieutenant, Civil Engineer Corps, U. S. Navy.

[redacted]